SLAC-PUB-2192
August 1978
(T/E)

QCD MODIFICATIONS OF THE 3-QUARK PICTURE OF A NUCLEON*

Francois Martin†
Stanford Linear Accelerator Center
Stanford University, Stanford, California 94305

ABSTRACT

Gluon bremsstrahlung processes inside the nucleon are investigated. A new method of inverting the moments is used which leads to analytic results for the parton distributions near $x = 1$ and $x = 0$. The 3-quark picture of the nucleon is studied with a minimum number of parameters or input. An "unrenormalized" valence quark distribution peaked at $x = \frac{1}{3}$, with a width related to the nucleon radius, and subsequently "renormalized" by gluon bremsstrahlung is in good agreement with deep inelastic data. However the gluon distribution obtained seems too steep near $x = 0$.

(Submitted to Phys. Rev. D)

---

*Work supported in part by the Department of Energy under Contract Number EY-76-C-03-0515.

†On leave of absence from LPTHE, Universities Paris VI and VII. Address after October 1, 1978: CERN, Geneva (Switzerland).

1. INTRODUCTION

The first runs of low energy eN and νN deep inelastic experiments ($E \lesssim 20$ GeV)[1,2] were in good agreement with Bjorken scaling. Later, more precise eN data[3] and high energy μN and νN experiments[4-8,15] have shown that there are actually small scaling violations. These violations appear to be in good agreement with asymptotically free gauge theories and more precisely with Quantum ChromoDynamics (QCD).[9-14,7]

The usual way to test QCD is to start with structure functions taken from the data at some $Q_0^2 \sim 4$ GeV^2 and then to study how QCD modifies these structure functions for $Q^2 > Q_0^2$. This scheme is in agreement with experiment but it involves a lot of parameters and unknown quantities, for example the shapes of the gluon and quark-antiquark sea distributions at Q_0^2. But it may be possible to go further by considering the nucleon as composed of 3 quarks bounded together via gluon exchanges and postulate that the glue and quark-antiquark sea actually "seen" inside the nucleon are produced only through gluon bremsstrahlung. This is very appealing because far fewer parameters and almost no data input are involved. In principle in this framework, using QCD, one should be able to predict completely the gluon and sea distributions. The only problem is that one has to choose the normalization point Q_0^2 in a region where perturbative QCD is not valid ($Q_0^2 \sim 0.1$ GeV^2). This picture has been suggested by many people[16-19] and will be fully developed in this paper.

The purpose of this paper is twofold. First, some general results on the variation of the structure functions with Q^2 are derived. In this respect the equations which describe the variation of parton densities with Q^2[20] are reviewed in Section 2. It appears that given boundary

conditions (at Q_0^2) the best way to solve these equations is to consider the Mellin transforms of the parton densities, i.e., the usual moments of the operator product expansion and renormalization group formalism.[10] A new method of inverting the moments is proposed which is very useful in order to obtain analytical results. For general boundary conditions the solutions are studied analytically near $x = 1$ and $x = 0$ (Section 3). Near $x = 1$ the valence, glue, and sea distributions $xV(x,Q^2)$, $xG(x,Q^2)$ and $xq_s(x,Q^2)$ behave like $(1 - x)^{v(Q^2)}$, $(1 - x)^{g(Q^2)}$ and $(1 - x)^{q_s(Q^2)}$, respectively,[21] QCD giving some relations between the powers $v(Q^2)$, $g(Q^2)$ and $q_s(Q^2)$. Some of these relations have been already discussed in References 22 and 23. As a result it is found that these dominant terms are good approximations of the exact solution only very near $x = 1$ and should not be extended on the entire $0 < x \leq 1$ range. Moreover, the range of dominance of some of those terms near $x = 1$ is appreciable only for $Q^2 >> Q_0^2$. Whatever is the behaviour of $xV(x,Q_0^2)$ near $x = 0$ it is found that for $Q^2 > Q_0^2$, $V(x,Q^2)$ goes to infinity as x goes to zero. It is also found that for $Q^2 > Q_0^2$ as x goes to zero, $xG(x,Q^2)$ and $xq_s(x,Q^2)$ go to infinity faster than any power of $\log \frac{1}{x}$ but slower than any $x^{-\varepsilon}$ power.[24]

The second part of this paper (Section 4) is devoted to the 3-quark picture mentioned above. The boundary conditions are then $G(x,Q_0^2) = q_s(x,Q_0^2) = 0$ with $V(x,Q_0^2)$ taken either from a harmonic oscillator quark model of the nucleon[16,17] or from a field theory with vector gluon exchange.[25] The results are compared with deep inelastic data. As far as the valence distribution is concerned the agreement is very good for both the x and Q^2 dependences. On the other hand, the gluon

distribution obtained seems too steep near $x = 0$. This last result comes mainly from a comparison with a measurement of gluon moments.[26]

Conclusions on this analysis are given in Section 5.

2. EQUATIONS DESCRIBING THE VARIATION OF PARTON DENSITIES WITH Q^2

A current with square momentum transfer $-Q^2 < 0$ which investigates the inside of a hadron can "see" a quark q_i or a gluon G,[27] which is then considered as a constituent of the struck hadron. $q_i(x,Q^2)$ and $G(x,Q^2)$ will respectively denote the densities of quark q_i and gluon G carrying a fraction x of the total longitudinal momentum of the hadron in the infinite momentum frame. In any renormalizable quark-gluon field theory in which perturbation theory is valid, the equations describing the variation of those parton densities with Q^2 are:[20,28]

$$\frac{\partial q_i(x,Q^2)}{\partial \log Q^2} = \frac{\alpha(Q^2)}{2\pi}\int_x^1 \frac{dy}{y}\left[P_{qq}\left(\frac{x}{y}\right)q_i(y,Q^2) + P_{qG}\left(\frac{x}{y}\right)G(y,Q^2)\right]$$

$$\frac{\partial G(x,Q^2)}{\partial \log Q^2} = \frac{\alpha(Q^2)}{2\pi}\int_x^1 \frac{dy}{y}\left[P_{Gq}\left(\frac{x}{y}\right)\sum_{i=1}^{2f} q_i(y,Q^2) + P_{GG}\left(\frac{x}{y}\right)G(y,Q^2)\right] \qquad (1)$$

$\alpha(Q^2)$ is the running coupling constant of quark-gluon interaction and f is the number of quark flavors. These equations account for all orders in $\alpha(Q^2)\log Q^2$ but only for first order in $\alpha(Q^2)$. They are typical of a shower phenomena. For an electromagnetic shower we have similar equations in which quark and gluon densities are respectively replaced by electron and photon densities.[29]

In QCD where the gauge group is SU(3) color, when $\alpha(Q^2)$ is small compared to 1, it is approximately given by

$$\alpha(Q^2) \approx \frac{12\pi}{(33 - 2f) \log \frac{Q^2}{\Lambda^2}} \tag{2}$$

where Λ gives the normalization of $\alpha(Q^2)$ at a fixed value of Q^2 (from experiment $\Lambda \sim 500$ MeV).

Let us now discuss the various functions $p_{ij}(z)$ of Eqs. (1). $p_{qq}\left(\frac{x}{y}\right)$ is given by diagram (a) of Fig. 1:

$$p_{qq}(z) = \frac{4}{3}\left[\frac{2}{(1 - z)_+} - (1 + z) + \frac{3}{2}\delta(z - 1)\right] \tag{3a}$$

where $\frac{1}{(1 - z)_+}$ is the following distribution

$$\int_0^1 dz \frac{f(z)}{(1 - z)_+} \equiv \int_0^1 dz \left[\frac{f(z) - f(1)}{1 - z}\right]$$

For comparison, in Quantum ElectroDynamics (QED)

$$p_{ee}(z) = \frac{2}{(1 - z)_+} - (1 + z) + \frac{3}{2}\delta(z - 1)$$

$p_{qG}\left(\frac{x}{y}\right)$ is given by diagram (b) of Fig. 1:

$$p_{qG}(z) = \frac{1}{2}\left[(1 - z)^2 + z^2\right] \tag{3b}$$

In QED

$$p_{e\gamma}(z) = (1 - z)^2 + z^2$$

$p_{Gq}\left(\frac{x}{y}\right)$ is given by diagram (c) of Fig. 1:

$$p_{Gq}(z) = \frac{4}{3}\left[\frac{1 + (1 - z)^2}{z}\right] \tag{3c}$$

In QED

$$p_{\gamma e}(z) = \frac{1 + (1 - z)^2}{z}$$

$P_{GG}\left(\frac{x}{y}\right)$ is given by diagram (d) of Fig. 1 (plus a contribution from diagram (b)):

$$P_{GG}(z) = 6\left[\frac{1}{(1-z)_+} + \frac{1}{z} - 2 + z(1-z) + \frac{(33-2f)}{36}\,\delta(z-1)\right] \qquad (3d)$$

In QED where there is no such 3γ coupling:

$$P_{\gamma\gamma}(z) = -\frac{2}{3}\,\delta(z-1)$$

Equations (1) can be rewritten in two steps: first by changing the variable $\log Q^2$ into

$$t = \frac{16}{(33-2f)}\log\left(\frac{\alpha(Q_0^2)}{\alpha(Q^2)}\right) \quad ; \qquad (4)$$

second by making a separation between valence and sea quarks

$$u(x,Q^2) = u_v(x,Q^2) + u_s(x,Q^2)$$

$$d(x,Q^2) = d_v(x,Q^2) + d_s(x,Q^2)$$

where

$$u_s(x,Q^2) = \bar{u}(x,Q^2)$$

$$d_s(x,Q^2) = \bar{d}(x,Q^2)$$

Thus when $\alpha(Q^2)$ is small compared to 1, and given by formula (2), Eqs. (1) read:

$$\frac{\partial}{\partial t}\,q_v(x,Q^2) = \int_x^1 \frac{dy}{y}\,f_{qq}\left(\frac{x}{y}\right)q_v(y,Q^2) \qquad (5a)$$

$$\frac{\partial}{\partial t}\,q_s(x,Q^2) = \int_x^1 \frac{dy}{y}\left[f_{qq}\left(\frac{x}{y}\right)q_s(y,Q^2) + f_{qG}\left(\frac{x}{y}\right)G(y,Q^2)\right] \qquad (5b)$$

$$\frac{\partial}{\partial t}\,G(x,Q^2) = \int_x^1 \frac{dy}{y}\left[f_{Gq}\left(\frac{x}{y}\right)\sum_{i=1}^{2f} q_i(y,Q^2) + f_{GG}\left(\frac{x}{y}\right)G(y,Q^2)\right] \qquad (5c)$$

where

$$q_v = u_v \text{ or } d_v$$

$$q_s = u_s(=\bar{u}),\ d_s(=\bar{d}), s, \bar{s}, c, \bar{c}, \ldots$$

$$f_{ij}(z) = \frac{3}{8} p_{ij}(z)$$

Note that in these equations quarks and gluons are treated as massless particles, which means that mass effects are not taken into account. Equation (5a) is satisfied by any difference of quark densities ($u_v = u - \bar{u}$, $u - s, \ldots$). This equation is decoupled from the others because the evolution with Q^2 of valence quark densities is governed only by gluon bremsstrahlung (Fig. 1a). In the Operator Product Expansion and Renormalization Group formulation of asymptotic freedom effects[10] this is known as the evolution with Q^2 of valence quark densities and is governed only by flavor non-singlet operators. Equations (5b) and (5c) are coupled (in the other formulation known as mixing of flavor singlet and non-singlet operators) because a) sea quarks are produced by pairs from gluons (Fig. 1b) and lose momentum by gluon bremsstrahlung (Fig. 1a); b) gluons are produced by gluon bremsstrahlung (Fig. 1c), are destroyed when they produce $q\bar{q}$ pairs (Fig. 1b), and can generate themselves (Fig. 1d).

Solving Eqs. (5a) through (5c) requires the knowledge of boundary conditions. If we know $q_v(x,Q_0^2)$, $q_s(x,Q_0^2)$ and $G(x,Q_0^2)$ for some Q_0^2 such that $\frac{\alpha(Q_0^2)}{\pi} << 1$, then Eqs. (5a) through (5c) enable us to know $q_v(x,Q^2)$, $q_s(x,Q^2)$ and $G(x,Q^2)$ for all values of Q^2 for which Eqs. (5a) through (5c) are valid (i.e., for $\frac{\alpha(Q^2)}{\pi} << 1$). The solutions of these equations are obtained by considering the Mellin transform of the quark and gluon densities:

$$M_j(s,Q^2) = \int_0^1 dx\, x^{s-1}\, j(x,Q^2)$$

where

$$j = q_v, q_s, G, \ldots$$

Equations (5a) through (5c) become

$$\frac{\partial}{\partial t} M_{q_v}(s,Q^2) = A_{qq}(s)\, M_{q_v}(s,Q^2) \tag{6a}$$

$$\frac{\partial}{\partial t} M_{q_s}(s,Q^2) = A_{qq}(s)\, M_{q_s}(s,Q^2) + A_{qG}(s)\, M_G(s,Q^2) \tag{6b}$$

$$\frac{\partial}{\partial t} M_G(s,Q^2) = A_{Gq}(s) \sum_{i=1}^{2f} M_{q_i}(s,Q^2) + A_{GG}(s)\, M_G(s,Q^2) \tag{6c}$$

where

$$A_{ij}(s) = \int_0^1 dz\, z^{s-1}\, f_{ij}(z)$$

From formulae (3) we get

$$A_{qq}(s) = \frac{3}{4} + \frac{1}{2s} - \frac{1}{2(s+1)} - \psi(s+1) - C \tag{7a}$$

$$A_{qG}(s) = \frac{3(2 + s + s^2)}{16s(s+1)(s+2)} \tag{7b}$$

$$A_{Gq}(s) = \frac{(2 + s + s^2)}{2s(s^2 - 1)} \tag{7c}$$

$$A_{GG}(s) = \frac{9}{4}\left[\frac{33 - 2f}{36} + \frac{1}{s-1} - \frac{1}{s} + \frac{1}{s+1} - \frac{1}{s+2} - \psi(s+1) - C\right] \tag{7d}$$

where $\psi(s+1) = \frac{\Gamma'(s+1)}{\Gamma(s+1)}$ is the digamma function $\left(= -C + \sum_{j=1}^{s} \frac{1}{j}\right.$ if s is a positive integer) and C is Euler's constant, C = 0.577... . Up to a multiplicative factor the A's are the usual anomalous dimensions found

in QCD.[10] It is now easy to solve Eqs. (6a) through (6c). The solution of Eq. (6a) is

$$M_{q_v}(s,Q^2) = M_{q_v}(s,Q_0^2)\, e^{t\, A_{qq}(s)}$$

$$= M_{q_v}(s,Q_0^2)\left[\frac{\log \frac{Q^2}{\Lambda^2}}{\log \frac{Q_0^2}{\Lambda^2}}\right]^{\frac{16}{(33-2f)}\, A_{qq}(s)} \tag{8a}$$

Solutions of Eqs. (6b) and (6c) are obtained after diagonalization and can be written in the following way

$$M_G(s,Q^2) = \left[M_v(s,Q_0^2) + 2f\, M_{q_s}(s,Q_0^2)\right] F_{Gq}(s,t) + M_G(s,Q_0^2) F_{GG}(s,t) \tag{8b}$$

$$M_{q_s}(s,Q^2) = M_v(s,Q_0^2) F_{q_s v}(s,t)$$

$$+ M_G(s,Q_0^2) F_{q_s G}(s,t) + M_{q_s}(s,Q_0^2) F_{q_s q_s}(s,t) \tag{8c}$$

This is for f flavors of quarks; quarks and gluons being treated as massless particles and the sea being SU(f) symmetric:

$$M_v(s,Q_0^2) = M_{u_v}(s,Q_0^2) + M_{d_v}(s,Q_0^2) \quad .$$

$F_{ij}(s,t)$ are known functions of t and of the A's which are given in Appendix I.

Having solved the equations satisfied by the Mellin transforms, we have to get back to the x distributions by computing the inverse Mellin transforms:

$$j(x,Q^2) = \frac{1}{2\pi i} \int_{c-i\infty}^{c+i\infty} ds\; x^{-s}\; M_j(s,Q^2) \tag{9}$$

where the contour $(c-i\infty,\ c+i\infty)$ is at the right of all singularities of $M_j(s,Q^2)$ in the complex s plane (Fig. 2). This method will be used to

obtain general results on the parton densities, assuming some general boundary conditions (Section 3). There is another way of computing the inverse Mellin transform which will be used in Section 4 dealing with the 3-quark picture. This method consists in computing the inverse Mellin transforms of the functions $F_{ij}(s,t)$: $\tilde{F}_{ij}(x,t)$, and then using the convolution formula equivalent to the product of Mellin transforms,[30,31] e.g.:

$$q_v(x,Q^2) = \int_x^1 \frac{dy}{y}\, q_v\left(\frac{x}{y},Q_0^2\right)\tilde{F}_{vv}(y,t) \qquad (10)$$

where $\tilde{F}_{vv}$ is the inverse Mellin transform of $F_{vv}(s,t) = e^{tA_{qq}(s)}$. Let us note that $\tilde{F}_{ij}(x,t)$ represents the x density of parton i found inside a parton j for a value $-Q^2$ of the square momentum transfer, the parton j being considered as a bare particle when the transfer is $-Q_0^2$. These functions $\tilde{F}_{ij}(x,t)$ can directly be used in processes which do not involve composite hadrons but quarks or gluons in the first place, e.g., e^+e^- annihilation.

3. GENERAL BOUNDARY CONDITIONS

In this section we shall discuss the behaviour of the quark and gluon densities near x = 1 and x = 0 corresponding to some general behaviour of the boundary densities.

3.1 Behaviour near x = 1

To study the behaviour of a parton density near x = 1 is equivalent to studying the limit of its Mellin transform for s going to infinity. Therefore if we make a $\frac{1}{s}$ expansion of its Mellin transform and compute the inverse Mellin transform of each term, we obtain an expansion of the

parton density near x = 1. Let's assume that the behaviour of the quark and gluon densities near x = 1 for $Q^2 = Q_0^2$ are

$$xV(x,Q_0^2) \sim K_v(1 - x)^v$$

$$xG(x,Q_0^2) \sim K_G(1 - x)^g$$

$$xq_s(x,Q_0^2) \sim K_{q_s}(1 - x)^{q_s}$$

Using formulae (7a) and (8a) and the fact that one can write

$$\psi(s + 1) = \log s + \frac{1}{2s} - \sum_{n=1}^{\infty} \frac{B_{2n}}{2n\, s^{2n}}$$

where B_n are Bernoulli numbers we obtain:

$$xV(x,Q^2) \sim K_v(Q^2)(1 - x)^{v(Q^2)} \tag{11}$$

where

$$v(Q^2) = v + t$$

and

$$K_v(Q^2) = K_v\, e^{t\left[\frac{3}{4} - c\right]} \frac{\Gamma(v + 1)}{\Gamma(v + 1 + t)}$$

This result is also given in References 31 and 22 but let us note that by making a $\frac{1}{s}$ expansion of the Mellin transform we obtain not only the dominant term near x = 1 but a whole expansion valid on the $0 < x \leq 1$ range.

For the gluon density $xG(x,Q^2)$, using formula (8b) and formulae (I.2) of Appendix I we get four dominant terms near x = 1. The first one corresponds to the glue produced by the valence quarks through bremsstrahlung. Near x = 1 it is equivalent to

$$K_{Gv}(Q^2)\frac{(1-x)^{(v+1+t)}}{\left[\log\frac{1}{1-x}+\psi(v+2+t)+\lambda\right]} \tag{12}$$

where

$$K_{Gv}(Q^2) = \frac{2}{5}K_v e^{t\left[\frac{3}{4}-c\right]}\frac{\Gamma(v+1)}{\Gamma(v+2+t)}$$

$$\lambda = c - \frac{21-2f}{20}$$

The second term corresponds to the glue radiated by the sea quarks. It is similar to the first term; near x = 1 it is equivalent to

$$K_{Gq_s}(Q^2)\frac{(1-x)^{(q_s+1+t)}}{\left[\log\frac{1}{1-x}+\psi(q_s+2+t)+\lambda\right]}$$

where

$$K_{Gq_s}(Q^2) = \frac{4f}{5}K_{q_s}e^{t\left[\frac{3}{4}-c\right]}\frac{\Gamma(q_s+1)}{\Gamma(q_s+2+t)}$$

The third term corresponds to the glue radiated by the glue itself. Near x = 1 it is equivalent to

$$K_{GG}^{(1)}(Q^2)(1-x)^{(g+\frac{9}{4}t)}$$

where

$$K_{GG}^{(1)}(Q^2) = K_G \exp\left[t\left(\frac{33-2f}{16}-\frac{9}{4}c\right)\right]\frac{\Gamma(g+1)}{\Gamma(g+1+\frac{9}{4}t)}$$

The last term corresponds to a gluon which creates a quark-antiquark pair which itself radiates glue. Near x = 1 it is equivalent to

$$K_{GG}^{(2)}(Q^2)\frac{(1-x)^{(g+2+t)}}{\left[\log\frac{1}{1-x}+\psi(g+3+t)+\lambda\right]^2}$$

where

$$K_{GG}^{(2)}(Q^2) = \frac{3f}{25}K_G e^{t\left[\frac{3}{4}-c\right]}\frac{\Gamma(g+1)}{\Gamma(g+3+t)}$$

Let us note that the power $(1 - x)^t$ comes from the summation of an infinite number of soft gluons radiated by a quark. On the other hand, the power $(1 - x)^{\frac{9}{4}t}$ comes from the summation of an infinite number of soft gluons radiated by a gluon. If we leave the $\log \frac{1}{1 - x}$ aside and say that near $x = 1$ the gluon density $xG(x,Q^2)$ behaves approximately like $(1 - x)^{g(Q^2)}$ then $g(Q^2)$ will be the smallest power of the 4 written above. We then have the following inequaling:[23]

$$g(Q^2) \leq v + 1 + t = v(Q^2) + 1$$

Similarly for the sea quark density $xq_s(x,Q^2)$, using formulae (8c) and (I.2), we get three dominant terms near $x = 1$. The first one corresponds to a $q\bar{q}$ pair produced from a valence quark through gluon radiation. Near $x = 1$ it is equivalent to

$$K_{q_s v}(Q^2) \frac{(1 - x)^{(v + 2 + t)}}{\left[\log \frac{1}{1 - x} + \psi(v + 3 + t) + \lambda\right]} \tag{13}$$

where

$$K_{q_s v}(Q^2) = \frac{3}{40} K_v t e^{t\left[\frac{3}{4} - c\right]} \frac{\Gamma(v + 1)}{\Gamma(v + 3 + t)}$$

The second term corresponds to a $q\bar{q}$ pair produced from the glue. Near $x = 1$ it is equivalent to

$$K_{q_s G}(Q^2) \frac{(1 - x)^{(g + 1 + t)}}{\left[\log \frac{1}{1 - x} + \psi(g + 2 + t) + \lambda\right]}$$

where

$$K_{q_s G}(Q^2) = \frac{3}{20} K_G e^{t\left[\frac{3}{4} - c\right]} \frac{\Gamma(g + 1)}{\Gamma(g + 2 + t)}$$

The third term corresponds simply to a sea quark which modifies its momentum by radiating glue. Near $x = 1$ it is equivalent to

$$K_{q_s q_s}(Q^2)(1 - x)^{(q_s + t)}$$

where

$$K_{q_s q_s}(Q^2) = K_{q_s} e^{t\left[\frac{3}{4} - c\right]} \frac{\Gamma(q_s + 1)}{\Gamma(q_s + 1 + t)}$$

If we leave the $\log \frac{1}{1 - x}$ aside and say that near $x = 1$ the sea density $xq_s(x,Q^2)$ behaves approximately like $(1 - x)^{q_s(Q^2)}$ then $q_s(Q^2)$ will be the smallest power of the three written above. We then have the following inequality:[23]

$$q_s(Q^2) \leq v + 2 + t = v(Q^2) + 2$$

Regarding the boundary powers v, g, and q_s, we have to consider two cases. The first one is for $g \geq v - 1$ and $q_s \geq v$; in this case we obtain the following relations[32]

$$g(Q^2) = v(Q^2) + 1$$

$$v(Q^2) \leq q_s(Q^2) \leq v(Q^2) + 2$$

The other case is for $g < v + 1$ or $q_s < v$ for which we have

$$g(Q^2) = q_s(Q^2) + 1 < v(Q^2) + 1$$

But usually the boundary powers are such that $g \geq v + 1$ and $q_s \geq v + 2$. In this case we have the following relations

$$g(Q^2) = v(Q^2) + 1$$

$$q_s(Q^2) = v(Q^2) + 2$$

or equivalently, near $x = 1$ the gluon and sea densities are dominated by the terms (12) and (13), respectively. This means that for Q^2 sufficiently larger than Q_0^2 the valence quarks generate most of the glue and sea quarks "seen" near $x = 1$. But let us note that this is true only in

the vicinity of $x = 1$ and the closer Q^2 is to Q_0^2 the smaller is the region of dominance of the terms (12) and (13) around $x = 1$. In other words, we should not extend these results on the entire [0,1] interval by saying, for example, that for $0 < x \leq 1$ the shape of the gluon distribution is $(1 - x)^{(v(Q^2) + 1)}$. This is shown in Section 4 and it means that for $0 < x \leq 1$ we have to take all the terms into account, and not only the ones that are dominant near $x = 1$.

3.2 Behaviour near $x = 0$

To study the behaviour of a parton density near $x = 0$ is equivalent to studying the behaviour of its Mellin transform near its rightmost singularity in the complex s plane. Therefore if we compute the contribution of each singularity of the Mellin transform, starting with the rightmost ones and using formula (9) integrated on the contour $\mathscr{C}$ of Fig. 2, we obtain an expansion of the parton density near $x = 0$.

Let us note, as an example, that the function $A_{qq}(s)$ has a pole at $s = 0 : \frac{1}{2s}$, which leads to an essential singularity at $s = 0$ for the function $F_v(s,t) = e^{t A_{qq}(s)} : e^{\frac{t}{2s}}$.

Let us assume that the behaviour of the quark and gluon densities near $x = 0$ for $Q^2 = Q_0^2$ are

$$xV(x,Q_0^2) \sim H_v x^r$$

$$xG(x,Q_0^2) \sim H_g$$

$$xq_s(x,Q_0^2) \sim H_{q_s}$$

For the valence density $xV(x,Q^2)$ we need to distinguish three cases:

a) $0 < r < 1$:[33] The rightmost singularity of $M_V(s,Q^2)$ is a pole at $s = 1 - r$, therefore using formula (8a), we obtain the following behaviour near $x = 0$

$$xV(x,Q^2) \sim H_V e^{t A_{qq}(1-r)} x^r$$

So in this case the x^r behaviour is stable under Q^2 variation. Regge pole arguments suggest $r = \frac{1}{2}$ which falls in this category and for which[24,22]

$$xV(x,Q^2) \sim H_V \exp\left[t\left(-\frac{7}{12} + 2\log 2\right)\right]\sqrt{x}$$

b) $r = 1$: The rightmost singularity of $M_V(s,Q^2)$ is an essential singularity at $s = 0$, therefore near $x = 0$ for $Q^2 > Q_0^2$

$$xV(x,Q^2) \sim H_V^{(1)}(Q^2)\, x\, I_0\left(\sqrt{2t\log\frac{1}{x}}\right)$$

$$\sim \frac{H_V^{(1)}(Q^2)}{\sqrt{2\pi}} \frac{x}{\left(2t\log\frac{1}{x}\right)^{1/4}} \exp\left(\sqrt{2t\log\frac{1}{x}}\right)$$

where $H_V^{(1)}(Q^2) = H_V e^{\frac{t}{4}}$ and $I_n(z)$ are the modified Bessel functions of the first kind.

c) $r > 1$: The rightmost singularity of $M_V(s,Q^2)$ is also an essential singularity at $s = 0$, therefore near $x = 0$ for $Q^2 > Q_0^2$

$$xV(x,Q^2) \sim H_V^{(2)}(Q^2)\, x \sqrt{\frac{t}{2\log\frac{1}{x}}}\, I_1\left(\sqrt{2t\log\frac{1}{x}}\right)$$

$$\sim \frac{H_V^{(2)}(Q^2)}{\sqrt{2\pi}} \frac{x\, t^{\frac{1}{4}}}{\left(2\log\frac{1}{x}\right)^{3/4}} \exp\left(\sqrt{2t\log\frac{1}{x}}\right)$$

where

$$H_v^{(2)}(Q^2) = e^{\frac{t}{4}} \int_0^1 \frac{dx}{x} V(x,Q_0^2)$$

In cases b) and c) when x goes to zero, $xV(x,Q^2)$ goes to zero slower than x but faster than any $x^{1-\varepsilon}$ power (with $\varepsilon > 0$), for $Q^2 > Q_0^2$. Therefore in these cases the x^r behaviour is not stable under Q^2 variation. Even if for $Q^2 = Q_0^2$, $xV(x,Q^2)$ has not a vertical tangent at $x = 0$, it has a vertical tangent at $x = 0$ for any $Q^2 > Q_0^2$. This may mean that when we compute the gluon bremsstrahlung contribution (Fig. 3a) we are in fact also computing a part of the ρ exchange contribution which creates the $\sqrt{x}$ behaviour near $x = 0$ (Fig. 3b).

For the gluon density $xG(x,Q^2)$, using formulae (8b) and (I.1) of Appendix I, we get three dominant terms near $x = 0$. The first one corresponds to a gluon produced from a valence quark through all types of "tower" diagrams like the one of Fig. 4. Near $x = 0$, for $Q^2 > Q_0^2$, it behaves like

$$2\, h(Q^2) \sqrt{\frac{t}{\log \frac{1}{x}}}\; I_1\left(3\sqrt{t \log \frac{1}{x}}\right)$$

where

$$h(Q^2) = \exp\left[-t\left(\frac{33}{16} + \frac{f}{72}\right)\right]$$

Let us notice that this term does not depend on the behaviour of the boundary function $xV(x,Q_0^2)$ near $x = 0$, but only on the fact that $\int_0^1 dx\, V(x,Q_0^2) = 3$. The second term corresponds to the glue produced from a sea quark or antiquark through all types of "tower" diagrams. Near $x = 0$ it is equivalent to

$$\frac{8f}{9} H_{q_s} h(Q^2) I_0\left(3\sqrt{t \log \frac{1}{x}}\right)$$

The third term corresponds to the glue produced from a gluon also through all types of "tower" diagrams (Fig. 4). Near x = 0 it behaves like

$$H_g h(Q^2) I_0\left(3\sqrt{t \log \frac{1}{x}}\right)$$

For the sea density $xq_s(x,Q^2)$ we also get three terms corresponding to pair production from valence quarks, sea and gluon respectively, through all types of "tower" diagrams. Near x = 0, for $Q^2 > Q_0^2$, those three terms behave respectively like

$$\frac{h(Q^2)}{6} \frac{t}{\log \frac{1}{x}} I_2\left(3\sqrt{t \log \frac{1}{x}}\right)$$

$$\frac{2f}{27} H_{q_s} h(Q^2) \sqrt{\frac{t}{\log \frac{1}{x}}} I_1\left(3\sqrt{t \log \frac{1}{x}}\right)$$

and

$$\frac{H_g}{12} h(Q^2) \sqrt{\frac{t}{\log \frac{1}{x}}} I_1\left(3\sqrt{t \log \frac{1}{x}}\right)$$

We also obtain similar behaviour near x = 0 for $Q^2 > Q_0^2$ if the boundary conditions are such that for any $\varepsilon > 0$, $x^{1+\varepsilon} G(x,Q_0^2)$ and $x^{1+\varepsilon} q_s(x,Q_0^2)$ go to zero when x goes to zero. From these results we see that when x goes to zero for $Q^2 > Q_0^2$, $xG(x,Q^2)$ and $xq_s(x,Q^2)$ go to infinity faster than any power of $\log \frac{1}{x}$ but slower than any $x^{-\varepsilon}$ power (with $\varepsilon > 0$).[24] Therefore in this framework the fact that $xG(x,Q_0^2)$ and $xq_s(x,Q_0^2)$ go to constants when x goes to zero is not a property which is stable under Q^2 variation. If we relate these results with the limit of the total $\gamma^*(Q^2)p$ cross section at high energy, we find that this last quantity

violates the Froissart bound. This may be a consequence of the fact that in this scheme we have ignored all high order $\alpha(Q^2)$ terms which are not of the $\alpha(Q^2)$ log Q^2 type.[24] If we could take all the higher order terms into account (and even nonperturbative effects), the answer might correspond to a saturation of the Froissart bound; i.e., $xG(x,Q^2)$ and $xq_s(x,Q^2)$ behave like $\left(\log \frac{1}{x}\right)^2$ when x goes to zero.

4. THE 3-QUARK PICTURE OF THE NUCLEON

It is appealing to consider that all the glue and $q\bar{q}$ pairs "seen" in the nucleon are produced via gluon bremsstrahlung.[18,19] This means that for Q_0^2 of the order of $m_u^2 \sim \left(\frac{m_p}{3}\right)^2 = 0.1\ \text{GeV}^2$ the boundary conditions will be

$$xG(x,Q_0^2) = 0$$

$$xq_s(x,Q_0^2) = 0 \qquad (14)$$

But for such small values of Q^2 Eqs. (1) are not valid $\left(\frac{\alpha(Q_0^2)}{\pi} \sim 1\right)$. Anyway, in this section the "normalization" point Q_0^2 will be chosen in this region, together with the boundary conditions (14). This approximation will still be valid if the higher order corrections only modify the coefficient $\frac{\alpha(Q^2)}{2\pi}$ into a more general function $f(\alpha(Q^2))$ in the region where $\frac{\alpha(Q^2)}{\pi} \sim 1$. The variable through which the Q^2 dependence occurs is

$$t = \frac{16}{(33 - 2f)} \log\left(\frac{\alpha(Q_0^2)}{\alpha(Q^2)}\right)$$

or more generally

$$t = \frac{16}{(33 - 2f)} \log\left(\frac{K}{\alpha(Q^2)}\right) \qquad (15)$$

From the fact that $\int_0^1 F_2^{ep}(x)\,dx \simeq 0.16$ for $Q^2 \sim 4$ GeV^2, which means that approximately 50% of the proton momentum is carried by gluons, we conclude that $Q^2 \sim 4$ GeV^2 corresponds to $t \sim 1.3$. Using $\Lambda = 500$ MeV and three flavors of quarks this leads to $\frac{K}{\pi}$ or $\frac{\alpha(Q_0^2)}{\pi} \sim 1.44$.

Moreover, we need to know the "unrenormalized" valence distribution $xV(x,Q_0^2)$ corresponding to the diagrams included in the circled part of Fig. 5. $V(x,Q_0^2)$ must satisfy the following conditions: a) $V(x,Q_0^2)$ should be peaked at $x = \frac{1}{3}$, b) its width should be related to the nucleon radius, c) $\int_0^1 xV(x,Q_0^2)dx = 1$, which means that all the nucleon momentum is carried by the valence quarks, d) $\int_0^1 V(x,Q_0^2)dx = 3$, which means that there are three valence quarks, and finally e) $V(x,Q_0^2)$ should behave like $(1 - x)^3$ near $x = 1$ because of a quark counting rule.[34] A harmonic oscillator quark model of the nucleon gives[17,16]

$$V(x,Q_0^2) \simeq N \exp\left[-\frac{3}{2}R^2 m_N^2\left(x - \frac{1}{3}\right)^2\right] \tag{16a}$$

On the other hand a field theory with vector gluon exchange gives[25]

$$V(x,Q_0^2) \simeq \frac{N'}{\left[\left(x - \frac{1}{3}\right)^2 + \frac{3}{R^2 m_N^2}\right]^3} \tag{16b}$$

These distributions have to be slightly modified near $x = 1$ in order to behave like $(1 - x)^3$. m_N is the nucleon mass and R the nucleon radius which is of the order of 0.75 Fermi. As a result of the analysis done in this section the two functions (16a) and (16b) give almost the same quark and gluon densities, and this for slightly different values of R:

distribution (16a) with R = 0.5 Fermi, which is in good agreement with experimental data, corresponds to distribution (16b) with R = 0.7 Fermi.

There may be a way of formulating this 3-quark picture of the nucleon without considering small values of Q^2 for which Eqs. (1) are not valid. This is by saying that a good approximation of the nucleon for $Q^2 \geq 1$ GeV^2 is the one given in Fig. 5 which consists of a factorization of a gluon bremsstrahlung process (Eqs. (1)) with a gluon exchange process among the three valence quarks (boundary conditions (14) and (16)). The solution of this problem is obtained with the help of an "abstract" normalization point Q_0^2 or more generally, a parameter K which relates the scales of Q^2 and t. As far as the mathematics are concerned, this formulation is completely equivalent to the one described at the beginning of this section. And we see that the larger Q^2 is, the better this 3-quark picture should be.

In order to obtain the quark and gluon distributions $xV(x,Q^2)$, $xG(x,Q^2)$ and $xq_s(x,Q^2)$ we have to solve Eqs. (1) with boundary conditions (14) and (16). This is done by considering the Mellin transforms of these distributions, which are given by formulae (8). To get back to the x distributions we compute the inverse Mellin transforms of the functions $F_{ij}(s,t)$ (see Appendix II) and then use the convolution formula (10). Once we know the distributions $xV(x,Q^2)$, $xG(x,Q^2)$ and $xq_s(x,Q^2)$ we can compare them with deep inelastic experiments (Fig. 6). Let us note that this comparison should be done only in the region where the parton model is valid (i.e., for $\frac{\alpha(Q^2)}{\pi} \ll 1$ or equivalently $Q^2 \geq 1$ GeV^2). For large Q^2 the variable x of parton densities equals the experimental variable x:

$$x = \frac{Q^2}{2m_N(E - E')}$$

In fact this formula has to be modified by target or quark mass effects.[35]

The valence quark distribution $xV(x,Q^2)$ can be directly compared to

$$F_2^{ep}(x,Q^2) - F_2^{en}(x,Q^2) = \frac{1}{3} x\left[u_v(x,Q^2) - d_v(x,Q^2)\right]$$

or

$$x\, F_3^{\nu N}(x,Q^2) = x\left[u_v(x,Q^2) + d_v(x,Q^2)\right]$$

The other structure functions involve the sea quark distributions:

$$F_2^{eN}(x,Q^2) = \sum_{i=1}^{2f} e_i^2\, xq_i(x,Q^2)$$

$$= \frac{4}{9} x\left[u + \bar{u} + c + \bar{c}\right]_{(x,Q^2)} + \frac{1}{9} x\left[d + \bar{d} + s + \bar{s}\right]_{(x,Q^2)}$$

in the case of four quark flavors. If we neglect charm production in neutrino experiments and set the Cabibbo angle equal to zero:

$$F_2^{\nu N}(x,Q^2) = x\left[u + d + \bar{u} + \bar{d}\right]_{(x,Q^2)}$$

On the other hand if we assume a full charm production (neglecting charm quark mass effects) and a charm sea equal to the strange sea ($c(x,Q^2) = s(x,Q^2)$) we also have charge symmetry in neutrino experiments and

$$F_2^{\nu N}(x,Q^2) = x\left[u + d + \bar{u} + \bar{d} + 4s\right]_{(x,Q^2)}$$

At this point let us define exactly what are our inputs for comparison with experiments. Conditions (14) are used together with

$$xV(x,Q_0^2) = x\left[u_v(x,Q_0^2) + d_v(x,Q_0^2)\right]$$

$$= N_1\, x\, \exp\left[-\frac{3}{2} R^2 m_N^2\left(x - \frac{1}{3}\right)^2\right] + N_2\sqrt{x}\,(1 - x)^3$$

where R = 0.48 Fermi, N_1 = 4.43, N_2 = 0.53.[36]

As a first approximation we assume $u_v(x,Q^2) = 2d_v(x,Q^2)$, which is known not to be satisfied for x > 0.4. The relation between Q^2 and t is given by formulae (15) and (2) in which Λ = 500 MeV and K is determined by the fact that t = 1.3 for Q^2 = 4 GeV^2 (e.g., for f = 4, K = 4.15).

The first step of our comparison with experimental data deals with the moments of structure functions, which does not involve the difficult task of computing the inverse Mellin transforms. The best experimental results on the valence moments come from a study of Gargamelle and BEBC data on $xF_3^{\nu N}(x,Q^2)$.[7] Comparison between experimental data and our predictions is done in Table I and Fig. 7a; agreement between the two is very good. In addition the BEBC group extracts the gluon moments from measurements of $F_2^{\nu N}(x,Q^2)$. Comparison with our predictions is given in Table II; except for the second moment (n = 2) agreement between the two is not very good. But, on the other hand, if we directly compare our predictions with experimental results on the moments of $F_2^{\nu N}(x,Q^2)$, as done on Fig. 7b, we get a good agreement. This means that it is difficult to extract with a good precision the gluon moments from $F_2^{\nu N}(x,Q^2)$.[37] Anderson et al.,[26] have also extracted the gluon moments from electron and muon deep inelastic scattering measurements on hydrogen and deuterium. Their results are more precise than those in neutrino experiments and appear to be of the same order of magnitude as BEBC results. Agreement with our predictions is good for the second moment (their result for

$Q^2 = 5$ GeV^2 is approximately 0.43, to be compared with 0.45 of Table II), but it is bad for the 4th and 6th moments (our predictions are approximately an order of magnitude below the data). On the other hand, if we directly compare our predictions with the experimental results on the moments of the electromagnetic structure functions F_2 for hydrogen and deuterium we also get good agreement for the second moments, but for the 4th and 6th moments our predictions are systematically 10 to 20% below the data.[38] The conclusion of this analysis is that the shape of the gluon distribution obtained in this paper is much steeper near $x = 0$ than the real one.

Let us now compare our prediction for the second moment of the quark-anitquark sea with Gargamelle, BEBC and CDHS data. An analysis of Gargamelle data[2] which neglects charm production gives

$$\frac{\left[M_{\bar{u}} + M_{\bar{d}}\right](2,Q^2)}{\left[M_u + M_d + M_{\bar{u}} + M_{\bar{d}}\right](2,Q^2)} = 0.054 \pm 0.026$$

This number has to be compared with our prediction for $Q^2 = 4$ GeV^2 : 0.069. An analysis of CDHS data[8] gives

$$\frac{\left[M_{\bar{u}} + M_{\bar{d}} + 2M_{\bar{s}}\right](2,Q^2)}{\left[M_u + M_d + M_s + M_{\bar{u}} + M_{\bar{d}} + M_{\bar{s}}\right](2,Q^2)} = 0.16 \pm 0.02$$

which is in good agreement with our prediction for $Q^2 \sim 20$ GeV^2 : 0.18. Results from BEBC[7] assume charge symmetry which is not satisfied if there is substantial charm production. Their result is $\frac{\overline{Q}}{(Q + \overline{Q})} = 0.113 \pm 0.030$. If we neglect charm production, our prediction for this quantity is 0.10 for $Q^2 \sim 20$ GeV^2. On the other hand, if we assume charm production with

a strange sea equal to the charm sea in order to have charge symmetry, our prediction for this quantity becomes 0.17 for $Q^2 \sim 20$ GeV^2. The conclusion of this analysis is that we obtain very good results as far as the second moments of the quark-antiquark sea are concerned.

The second step of our comparison with experimental data deals with structure functions as functions of x and Q^2. First, using the results of Section 3.1, let us investigate the behaviour of these functions near $x = 1$. Near $x = 1$ the valence, gluon and sea distributions behave like $(1 - x)^{(3 + t)}$, $\frac{(1 - x)^{(4 + t)}}{|\log(1 - x)|}$ and $\frac{(1 - x)^{(5 + t)}}{|\log(1 - x)|}$, respectively. For $Q^2 = 4$ GeV^2 the powers are respectively 4.3, 5.3 and 6.3, which are good values. But let us recall that this result is valid only near $x = 1$ and should not be extrapolated for $0 < x \leq 1$. Near $x = 0$ the results are those of Section 3.2, i.e., a vertical tangent for $xV(x,Q^2)$ and gluon and sea distributions $xG(x,Q^2)$ and $xq_s(x,Q^2)$ which go to infinity. Figure 8 shows the shape of $xG(x,Q^2)$ for $Q^2 = 4$ GeV^2 and 20 GeV^2, respectively. It also shows a function $C^{st}(1 - x)^5$ normalized to the same area as $xG(x,Q^2 = 4 \text{ GeV}^2)$ for x between 0 and 1. So, even if $xG(x,Q^2 = 4 \text{ GeV}^2)$ behaves like $\frac{(1 - x)^{5.3}}{|\log(1 - x)|}$ near $x = 1$, it is a much steeper function than $(1 - x)^5$ on the entire $0 \leq x \leq 1$ interval. Figure 9 shows the shape of $xq_s(x,Q^2)$ also for $Q^2 = 4$ GeV^2 and 20 GeV^2, respectively. Comparison of $xq_s(x,Q^2 = 4 \text{ GeV}^2)$ with a function $C^{st}(1 - x)^7$ normalized to the same area for x between 0 and 1 shows that the sea distribution is steeper than $(1 - x)^7$ on the $0 \leq x \leq 1$ interval, even if near $x = 1$ it behaves like $\frac{(1 - x)^{6.3}}{|\log(1 - x)|}$.

Let us now compare Gargamelle data[2] on quark and antiquark distributions inside an isoscalar target, with our predictions of $xQ(x,Q^2) = x[u(x,Q^2) + d(x,Q^2)]$ and $x\bar{Q}(x,Q^2) = x[\bar{u}(x,Q^2) + \bar{d}(x,Q^2)]$ for $Q^2 = 4$ GeV^2. This is done in Fig. 10. Agreement is good for the quark distribution. For the antiquark distribution it is difficult to draw a definite conclusion because of poor statistics. Comparison of the BEBC data[7] on quark distribution with the curve which agrees with the Gargamelle quark distribution shows that there is definitely a shrinkage of this distribution when Q^2 increases (Fig. 11). There is good agreement between BEBC data and our predictions of $xQ(x,Q^2) = x[u(x,Q^2) + d(x,Q^2)]$ or $x[u(x,Q^2) + d(x,Q^2) + 2s(x,Q^2)]$[39] for $Q^2 = 20$ GeV^2. For the antiquark distribution it is difficult to draw a definite conclusion because of poor statistics. We investigate now SLAC[3] and FNAL[4] data on electron and muon deep inelastic scattering on hydrogen. These data refer to the structure function $F_2^{ep}(x,Q^2)$. They are more precise than those in neutrino experiments and are given for various Q^2 bins which is better for comparison with our predictions. Figures 12, 13 and 14 show this comparison for three different Q^2 bins. Our predictions are shown for 3 and 4 quark flavors[40] (a fifth bottom quark does not change appreciably the 4 flavor curves because of its $\frac{1}{3}$ electric charge). Agreement is good for $x < 0.4$ and suggests appreciable charm quark production (note that for $x = 0.1$ and $Q^2 = 4$ GeV^2 : $w^2 = 37$ GeV^2, which is well above the charm threshold). The relative poor agreement for $x > 0.4$ may have two causes. First, we did not account for target mass effects, which means that we should have used the scaling variable ξ instead of the variable x.[35] And above all, we have used the relation $u_v(x,Q^2) = 2\,d_v(x,Q^2)$ which is known

not to be satisfied for $x > 0.4$. Finally let us notice that from comparison of our predictions with data at low x there is no indication that the sea distribution obtained in this paper is too steep near $x = 0$.

5. CONCLUSIONS

The 3-quark picture of a nucleon certainly seems to have something to do with reality. It is found in this paper that an "unrenormalized" valence quark distribution peaked at $x = \frac{1}{3}$ and whose width is related to the nucleon radius with a value $R \sim 0.5 - 0.7$ Fermi, and which is subsequently modified by QCD gluon bremsstrahlung processes, gives in first approximation a good fit of the experimental valence quark distribution $xV(x,Q^2)$ for $Q^2 \geq 2$ GeV^2. Moreover, this model gives the right partition of momentum between quarks, gluons and antiquarks. This last fact was already pointed out in References 18 and 19, but the shape of the glue x distribution predicted in this model seems to be slightly different from the observed one.[41] It appears too steep near $x = 0$, a fact already noted in Reference 14. This last point is certainly related to the behaviour of those distributions near $x = 0$ which is found to violate the Froissart bound, a consequence of the intrinsic nature of Eqs. (1) and not of the 3-quark picture. So an improvement of this model probably lies in taking account of higher order terms like $\alpha(Q^2)(\alpha(Q^2)\log Q^2)^n$. There may also be an appreciable contribution from diagrams which are not specifically of the gluon bremsstrahlung type, like the ones in Fig. 15. Moreover, quark and gluon mass effects should be studied.

Let us emphasize that good agreement with deep inelastic data has been obtained with a minimum number of parameters or data input; in fact,

only three: the nucleon radius R, the parameter K of formula (15) which relates the Q^2 and t scales and finally Λ which controls the Q^2 variation.

Acknowledgment

I thank R. Blankenbecler for his considerable help during the course of this work and R. Staffin for his careful reading of the manuscript. I also acknowledge useful discussions with J. Bjorken, S. Brodsky, D. Coward, T. De Grand, A. De Rújula and J. Ellis. This work is supported in part by the Department of Energy.

APPENDIX I

Functions $F_{ij}(s,t)$ of formulae (8) are functions of t and of the $A_{kl}(s)$ given by formulae (7):

$$F_{VV}(s,t) = e^{tA_{qq}(s)}$$

$$F_{Gq}(s,t) = A_{Gq}(s)\, f(s,t)$$

$$F_{GG}(s,t) = \frac{1}{2}\left(A_{GG}(s) - A_{qq}(s)\right) f(s,t) + \frac{1}{2}\, g(s,t)$$

$$F_{q_s v}(s,t) = \frac{1}{2f}\left[-e^{tA_{qq}(s)} - \frac{1}{2}\left(A_{GG}(s) - A_{qq}(s)\right) f(s,t) + \frac{1}{2}\, g(s,t)\right]$$

$$F_{q_s q_s}(s,t) = -\frac{1}{2}\left(A_{GG}(s) - A_{qq}(s)\right) f(s,t) + \frac{1}{2}\, g(s,t)$$

$$F_{q_s G}(s,t) = A_{qG}(s)\, f(s,t)$$

where

$$f(s,t) = \frac{e^{t\lambda_+(s)} - e^{t\lambda_-(s)}}{\lambda_+(s) - \lambda_-(s)}$$

$$g(s,t) = e^{t\lambda_+(s)} + e^{t\lambda_-(s)} \qquad \text{(I.1)}$$

$$\lambda_\pm(s) = \frac{1}{2}\left[A_{GG}(s) + A_{qq}(s) \pm \sqrt{\left(A_{GG}(s) - A_{qq}(s)\right)^2 + 8f A_{Gq}(s) A_{qG}(s)}\right]$$

There is another way of writing the functions $F_{ij}(s,t)$, using the following formulae:

$$f(s,t) = \int_0^t dv \left[\sum_{n=0}^{\infty} U^n(s) \frac{v^n}{n!} \frac{(t-v)^n}{n!}\right] \exp\left[(t-v) A_{GG}(s) + v A_{qq}(s)\right]$$

$$F_{GG}(s,t) = e^{tA_{GG}(s)} + \int_0^t dv \left[\sum_{n=1}^{\infty} U^n(s) \frac{v^n}{n!} \frac{(t-v)^{(n-1)}}{(n-1)!}\right] \exp\left[v A_{GG}(s) + (t-v) A_{qq}(s)\right]$$

$$F_{q_s v}(s,t) = \frac{1}{2f} \int_0^t dv \left[\sum_{n=1}^{\infty} U^n(s) \frac{v^n}{n!} \frac{(t-v)^{(n-1)}}{(n-1)!}\right] \exp\left[(t-v) A_{GG}(s) + v A_{qq}(s)\right]$$

$$F_{q_s q_s}(s,t) = e^{tA_{qq}(s)} + 2f\, F_{q_s v}(s,t)$$

where

$$U(s) = 2f A_{Gq}(s)\, A_{qG}(s) \,. \qquad \text{(I.2)}$$

In these expansions the $U^n(s)$ term corresponds to a gluon produced from a gluon through the production of n quark-antiquark pairs (Fig. 4). This way of writing the functions $F_{ij}(s,t)$ is very useful when studying the behaviour of the parton densities near $x = 1$ (Section 3.1).

APPENDIX II

To solve the inverse Mellin transform problem with boundary conditions (14) and (16) and the use of formula (10) requires the computation of the inverse Mellin transforms of functions $F_{vv}(s,t)$, $F_{Gq}(s,t)$ and $F_{q_s v}(s,t)$ given in Appendix I.

1) $F_{vv}(s,t)$

Writing

$$\psi(s+1) = \log(s+1) - \frac{1}{2(s+1)} - \sum_{n=1}^{\infty} \frac{B_{2n}}{2n(s+1)^{2n}}$$

we obtain

$$F_{vv}(s,t) = e^{t\left[\frac{3}{4} - c\right]} \frac{e^{\frac{t}{2s}}}{(s+1)^t} \exp\left[t \sum_{n=1}^{\infty} \frac{B_{2n}}{2n(s+1)^{2n}}\right]$$

$$= e^{t\left[\frac{3}{4} - c\right]} e^{\frac{t}{2s}} \sum_{p=0}^{\infty} \frac{A_p(t)}{(s+1)^{(t+p)}}$$

Then we can write its inverse Mellin transform as

$$\tilde{F}_{vv}(x,t) = e^{t\left[\frac{3}{4} - c\right]} \sum_{p=0}^{\infty} Ap(t) f(t+p, \frac{t}{2}, x)$$

where $f(r,u,x)$ is the inverse Mellin transform of $\dfrac{e^{\frac{u}{s}}}{(s+1)^r}$.

$$f(r,u,x) = \sum_{p=0}^{\infty} \frac{u^p}{p!} \left(\log \frac{1}{x}\right)^{(r+p-1)} \frac{1}{\Gamma(r+p)} M(r, r+p, \log x)$$

where $M(a,b,z)$ is a confluent hypergeometric function.

$$M(a,b,z) = 1 + \sum_{k=1}^{\infty} \frac{z^k}{k!} \frac{a(a+1)\ldots(a+k-1)}{b(b+1)\ldots(b+k-1)}$$

These expansions correspond to the vicinity of x = 1, but they converge so well that it is possible to use them to compute $\tilde{F}_{VV}(x,t)$ even near x = 0 (e.g., for x = 0.01). Summing the various terms of these expansions is done by computer. Let us note that the different confluent hypergeometric functions involved are connected via a recursive formula:

$$y\,m\,M(t,\ t+m+1,\ -y) = (t+m)\left\{(t+m-1)\,M(t,\ t+m-1,\ -y) + (y-t-m+1)\,M(t,\ t+m,\ -y)\right\}$$

2) $F_{Gq}(s,t)$

To get an expansion of its inverse Mellin transform $\tilde{F}_{Gq}(x,t)$ near x = 1 we use formulae (I.2) of Appendix I. A $\frac{1}{(s-1)}$ expansion of the integrand:

$$A_{Gq}(s)\left[\sum_{n=0}^{\infty} U^n(s)\,\frac{v^n}{n!}\,\frac{(t-v)^n}{n!}\right]\exp\left[(t-v)\,A_{GG}(s) + v\,A_{qq}(s)\right]$$

is then done. Using the fact that the inverse Mellin transform of $\frac{1}{(s-1)^r}$ is $\frac{1}{x\Gamma(r)}\left(\log\frac{1}{x}\right)^{(r-1)}$ we obtain the Mellin transform of each term of the expansion. Finally $\tilde{F}_{Gq}(x,t)$ is obtained after integration over v. This method is used on the interval $0.6 \leqslant x \leqslant 1$.

For small values of x we start with formulae (I.1) of Appendix I that we rewrite as a t expansion:[42]

$$F_{Gq}(s,t) = \sum_{n=1}^{\infty} A_{Gq}(s)\,\frac{t^n}{n!}\left[\frac{\lambda_+^n(s) - \lambda_-^n(s)}{\lambda_+(s) - \lambda_-(s)}\right]$$

$$= \sum_{n=1}^{\infty} A_{Gq}(s)\,\frac{t^n}{n!}\,L_n(s)$$

We compute the contributions of all the singularities of $F_{Gq}(s,t)$ in the complex s plane: s = 1, 0, -1, -2,..., the various contributions being

computed in this order. This is done using the t expansion written above together with the following recursive formula

$$L_n(s) = \left(A_{GG}(s) + A_{qq}(s)\right) L_{n-1}(s) - \left(A_{GG}(s)\, A_{qq}(s) - 2fA_{Gq}(s)\, A_{qG}(s)\right) L_{n-2}(s),$$

with $L_0(s) = 0$ and $L_1(s) = 1$. Knowing that the inverse Mellin transform of $\frac{1}{(s+p)^r}$ is $\frac{x^p}{\Gamma(r)} \left(\log \frac{1}{x}\right)^{(r-1)}$ a computer is used to sum all the terms. This method is used on the interval $0 < x \leqslant 0.6$. We check that the two types of expansions described above give the same results for $x \sim 0.6$.

3) $F_{q_s v}(s,t)$

To get an expansion of its inverse Mellin transform $\widetilde{F}_{q_s v}(x,t)$ near $x = 1$ we use formulae (I.2) of Appendix I and the same method as for $F_{Gq}(s,t)$.

For small values of x we start with formulae (I.1) of Appendix I which we rewrite as a t expansion:

$$F_{q_s v}(s,t) = \frac{1}{2f} \sum_{n=2}^{\infty} \frac{t^n}{n!} P_n(s)$$

where $P_n(s)$ is given by

$$P_n(s) = U(s)\, A_{qq}^{n-2}(s) + \left(A_{GG}(s) + A_{qq}(s)\right) P_{n-1}(s) - \left(A_{GG}(s)\, A_{qq}(s) - U(s)\right) P_{n-2}(s)$$

with $P_1(s) = 0$, $P_2(s) = U(s)$. Then we proceed exactly as we did for $F_{Gq}(s,t)$.

REFERENCES

1. E. D. Bloom et al., Phys. Rev. Letters 23, 930 (1969); M. Breidenbach et al., Phys. Rev. Letters 23, 935 (1969).
2. H. Deden et al., Nucl. Phys. B85, 269 (1975).
3. E. M. Riordan et al., SLAC-PUB-1634 (1975); W. B. Atwood, Ph.D. Thesis, SLAC-Report-185 (1975).
4. H. L. Anderson et al., Phys. Rev. Letters 38, 1450 (1977); C. Chang et al., Phys. Rev. Letters 35, 901 (1975).
5. A. Benvenuti et al., Phys. Rev. Letters 36, 1478 (1976); 37, 189 (1976).
6. B. C. Barish et al., Phys. Rev. Letters 39, 1595 (1977).
7. P. C. Bosetti et al., Preprint OXFORD-NP-16/78.
8. M. Holder, talk presented at the SLAC Summer Institute on Particle Physics (July 1978).
9. Except for a large ratio σ_L/σ_T seen at SLAC and Fermilab [3, 15].
10. H. D. Politzer, Phys. Rev. Letters 30, 1346 (1973); D. J. Gross and F. Wilczek, ibid. 30, 1343 (1973).
11. A. De Rújula, H. Georgi and H. D. Politzer, Annals of Physics 103, 315 (1977).
12. G. Altarelli, R. Petronzio and G. Parisi, Phys. Letters 63B, 183 (1976); R. M. Barnett, H. Georgi and H. D. Politzer, Phys Rev. Letters 37, 1313 (1976); R. M. Barnett and F. Martin, Phys. Rev. D16, 2765 (1977); A. J. Buras, Nucl. Phys. B125, 125 (1977); C. C. Fox, Nucl. Phys. B134, 269 (1978).

13. A. J. Buras and K.J.F. Gaemers, Nucl. Phys. B132, 249 (1978); G. C. Fox B131, 107 (1977).

14. I. Hinchliffe and C. H. Llewellyn Smith, Nucl. Phys. B128, 93 (1977); Phys. Letters 70B, 247 (1977).

15. B. A. Gordon et al., Phys. Rev. Letters 41, 615 (1978).

16. G. Altarelli, N. Cabibbo, L. Maiani and R. Petronzio, Nucl. Phys. B69, 531 (1974).

17. A. Le Yaouanc, L. Oliver, O. Pène and J. C. Raynal, Phys. Rev. D12, 2137 (1975).

18. V. A. Novikov, M. A. Shifman, A. I. Vainshtein and V. I. Zakharov, Annals of Physics 105, 276 (1977); V. I. Zakharov, talk presented at the 18th Int. Conf. on High Energy Physics, Tbilisi, USSR, July 15-21, 1976.

19. G. Parisi and R. Petronzio, Phys. Letters 62B, 331 (1976).

20. G. Altarelli and G. Parisi, Nucl. Phys. B126, 298 (1977); G. Parisi, talk presented at the Intern. Meeting on Neutrino Physics, Flaine, March 6-12, 1976, published in Moriond Conf. page 83 (1976).

21. Except for some $1/|\log (1 - X)|$ factors.

22. N. Cabibbo and R. Petronzio, Nucl. Phys. B137, 395 (1978).

23. C. H. Llewellyn Smith and S. Wolfram, Nucl. Phys. B138, 333 (1978).

24. A. De Rújula et al., Phys. Rev. D10, 1649 (1974).

25. I. A. Schmidt and R. Blankenbecler, Phys. Rev. D15, 3321 (1977). See also T. N. Pham, SLAC-PUB-2172.

26. H. L. Anderson, H. S. Matis and L. C. Myrianthopoulos, Phys. Rev. Letters 40, 1061 (1978).

27. The electromagnetic and weak currents are not coupled to the gluon field but there exist other currents which are; e.g. the gluon current is coupled to the gluon field.

28. J. Kogut and L. Susskind, Phys. Rev. D9, 697 (1971).

29. Y. S. Tsai and Van Whitis, Phys. Rev. 149, 1248 (1966).

30. G. Parisi, Phys. Letters 43B, 207 (1973).

31. D. J. Gross, Phys. Rev. Letters 32, 1071 (1974).

32. These relations are slightly different from those obtained in ref. [23].

33. r has to be strictly positive in order for $V(x,Q_0^2)$ to be integrable near x = o.

34. S. D. Drell and T. M. Yan, Phys. Rev. Letters 24, 181 (1970); G. B. West, Phys. Rev. Letters 24, 1206 (1970).

35. O. Nachtmann, Nucl. Phys. B63, 237 (1973) and B78, 455 (1974); H. Georgi and H. D. Politzer, Phys. Rev. Letters 36, 1281 (1976) and 37, 68 (1976).

36. The N_2 term has been added to the N_1 term in order that $V(x,Q_0^2)$ satisfies the normalization conditions c) and d). It appears that for most of $0 \leq x \leq 1$ the N_2 term is much smaller than the N_1 term. In addition, this function $xV(x,Q_0^2)$ has to be modified near x = 1 in order to behave like $(1 - x)^3$ but this changes the results appreciably only in the region $0.9 \leq x \leq 1$.

37. Moreover we disagree with formula (18), which the BEBC group uses in order to extract the gluon moments from $F_2^{\nu N}(x,Q^2)$ (Ref. [7]).

38. Let us notice that the data do not cover the entire $0 \leq x \leq 1$ range for a fixed value of Q^2. In particular it is impossible to know the exact limit of $F_2(x,Q^2)$ when x goes to zero.

39. The difference between the two expressions consists in respectively not taking and taking account of charm production. In using the second expression we assume that the sea is SU(4) symmetric.

40. In each case the sea is respectively SU(3) and SU(4) symmetric.

41. This may also be true for the sea distribution.

42. A t expansion corresponds to a pertubative expansion in quark-gluon and gluon-gluon vertices.

TABLE 1

Comparison of BEBC results [7] with our predictions for the first five moments of the valence quark distribution for $Q^2 = 5\ GeV^2$ ($t = 1.35$).

n	Valence $M_v(n, Q^2 = 5\ GeV^2)$	
	BEBC	$t = 1.35$
1	$\geq 2.5 \pm 0.5$	3
2	$0.45 \pm .07$	0.41
3	$0.12 \pm .02$	0.12
4	$0.045 \pm .010$	0.047
5	$0.027 \pm .007$	0.022

TABLE 2

Comparison of BEBC results [7] with our predictions for the moments $n = 2 - 5$, of the gluon distribution for $Q^2 = 5\ GeV^2$ ($t = 1.35$). Errors in parentheses come from uncertainty in the value of Λ used by BEBC. The number in brackets ($n = 2$) has been deduced by BEBC from the nucleon momentum sum rule.

n	Glue $M_G(n, Q^2 = 5\ GeV^2)$	
	BEBC	$t = 1.35$
2	$0.62 \pm .15\ (.03)[0.45 \pm .03]$	0.45
3	$0.12 \pm .05\ (.02)$	0.026
4	$0.03 \pm .02\ (.015)$	0.0049
5	$0.02 \pm .01\ (.02)$	0.0014

FIGURE CAPTIONS

1. Diagrams leading to functions $p_{ij}\left(\frac{x}{y}\right)$ involved in equations (1).
2. Complex s plane.
3. Diagrams showing the analogy between gluon bremsstrahlung (a) and ρ exchange (b) contributions.
4. "Tower" diagram involving n quark-antiquark pairs.
5. A 3-quark picture of the nucleon.
6. Deep inelastic scattering of lepton ℓ (energy E) off nucleon target N; E' is the energy of outgoing lepton ℓ'.
7. a) Comparison of BEBC results [7] with our predictions (solid lines) for the first Nachtmann moments of $xF_3^{\nu N}(x,Q^2)$ versus Q^2.
   b) Comparison of BEBC results with our predictions (solid lines) for the first Nachtmann moments of $F_2^{\nu N}(x,Q^2)$ versus Q^2. For n = 2 the upper line takes account of charm production whereas the lower one does not. The higher moments are not appreciably modified by charm production.
8. Gluon distribution $xG(x,Q^2)$ as a function of x for $Q^2 = 4$ GeV^2 (t = 1.3, __) and $Q^2 = 20$ GeV^2 (t = 1.6, __.__). The dashed curve (___) is a function $C^{st}(1 - x)^5$ normalized to the same area as the solid curve for $0 \leq x \leq 1$.
9. Sea quark distribution $xq_s(x,Q^2)$ as a function of x for $Q^2 = 4$ GeV^2 (t = 1.3, __) and $Q^2 = 20$ GeV^2 (t= 1.6, __.__). The dashed curve (___) is a function $C^{st}(1 - x)^7$ normalized to the same area as the solid curve for $0 \leq x \leq 1$.
10. Comparison of Gargamelle results [2] on quark (✦) and antiquark (*) distributions with our predictions (solid lines) of these

quantities for $Q^2 = 4$ GeV^2 ($t = 1.3$) x' is the effective scaling variable used by Gargamelle and is considered equal to our variable x.

11. Comparison of BEBC results [7] on quark (♦) and antiquark (▲) distributions as functions of x for $Q^2 = 3 - 100$ GeV^2 with out predictions. The dashed dotted curve (-·-) is $x[u(x,Q^2) + d(x,Q^2)]$ for $Q^2 = 4$ GeV^2 ($t = 1.3$). The two upper solid lines are respectively $x[u + d]$ and $x[u + d + 2s]$ for $Q^2 = 20$ GeV^2 ($t = 1.6$). The two lower solid lines are respectively $x[\bar{u} + \bar{d}]$ and $x[\bar{u} + \bar{d} + 2\bar{s}]$ for $Q^2 = 20$ GeV^2 ($t = 1.6$).

12. Comparison of SLAC (△)[3] and FNAL (♦)[4] data on $F_2^{ep}(x,Q^2)$ and $F_2^{\mu p}(x,Q^2)$ respectively, with our predictions. SLAC data are for $Q^2 = 3$ GeV^2 and FNAL data for 2 GeV$^2 \leq Q^2 \leq 4$ GeV^2. Only statistical errors are shown. The lower solid curve does not include the charm quark sea whereas the upper solid curve does; both curves correspond to $Q^2 = 3$ GeV^2 ($t = 1.23$).

13. Same as figure 12. SLAC data are for $Q^2 = 6$ GeV^2 (except the point at $x = 0.25$ which is for $Q^2 = 5$ GeV^2) and FNAL data for 4 GeV$^2 \leq Q^2 \leq 8$ GeV^2. The curves are for $Q^2 = 6$ GeV^2 ($t = 1.39$).

14. Same as figure 12. SLAC data are for $Q^2 = 12$ GeV^2 and FNAL data for 8 GeV$^2 \leq Q^2 \leq 15$ GeV^2. The curves are for $Q^2 = 11.5$ GeV^2 ($t = 1.51$).

15. Some diagrams which have not been taken into account in the computation of sea quark and gluon distributions.

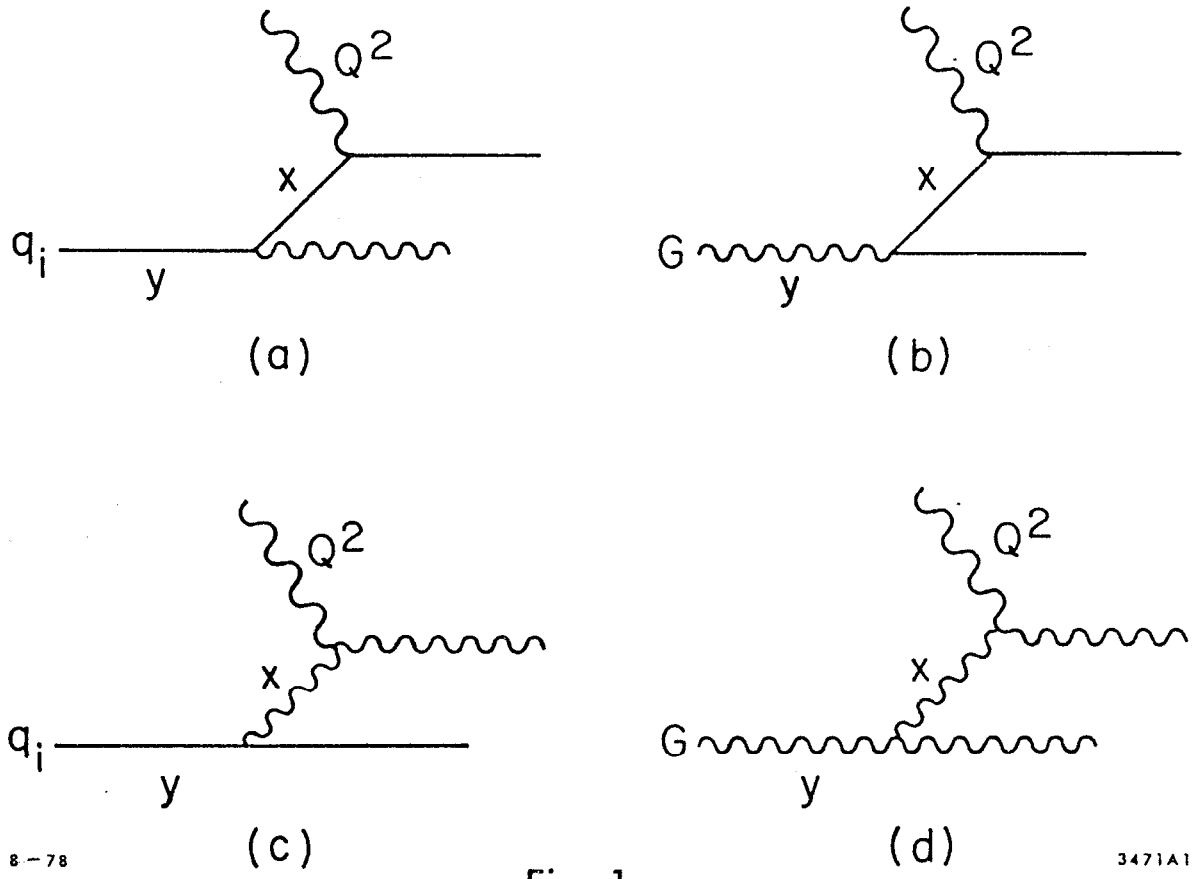

8-78

3471A1

Fig. 1

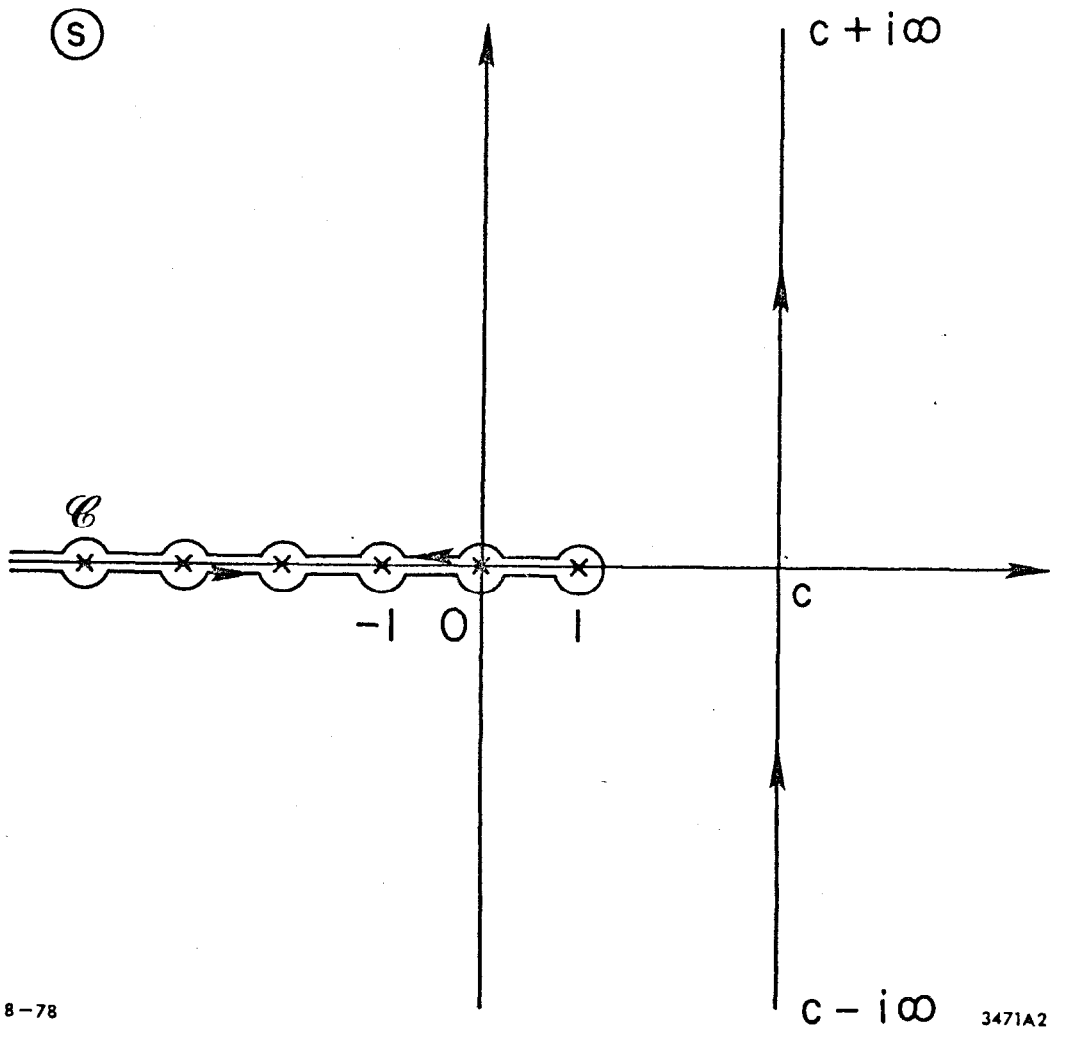

Fig. 2

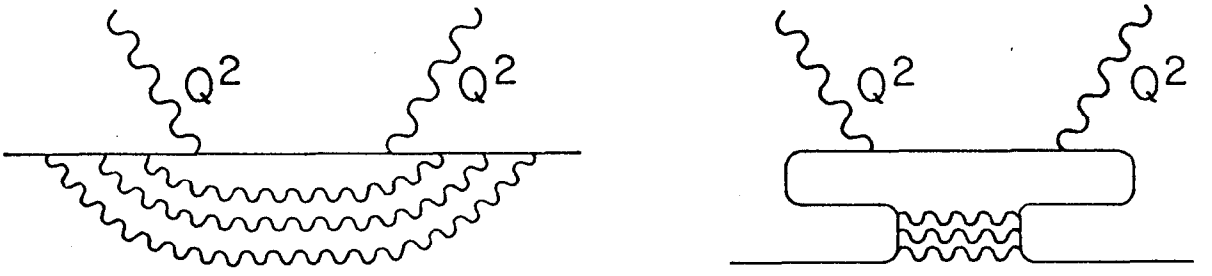

8-78 (a) (b) 3471A3

Fig. 3

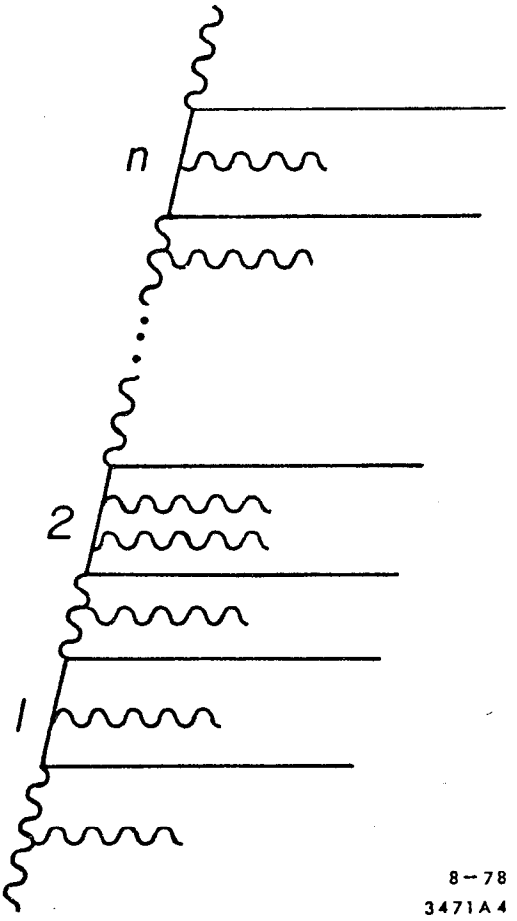

Fig. 4

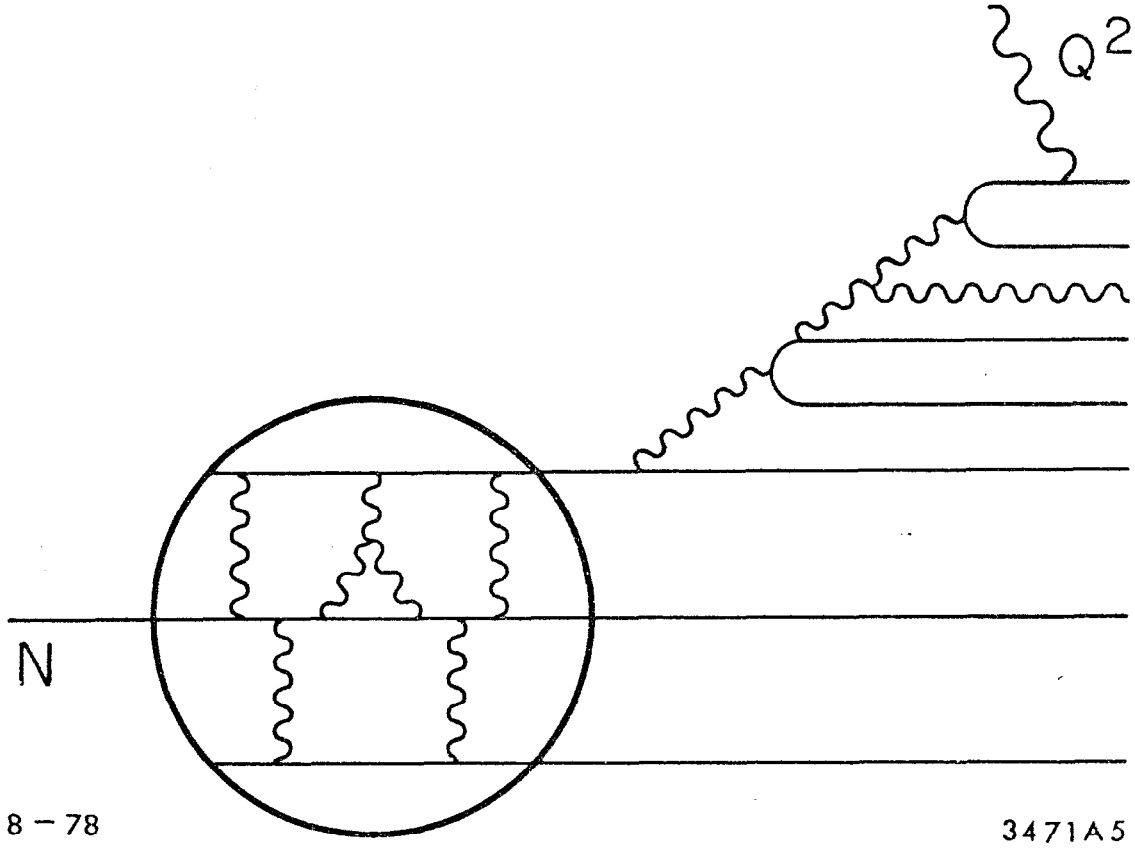

Fig. 5

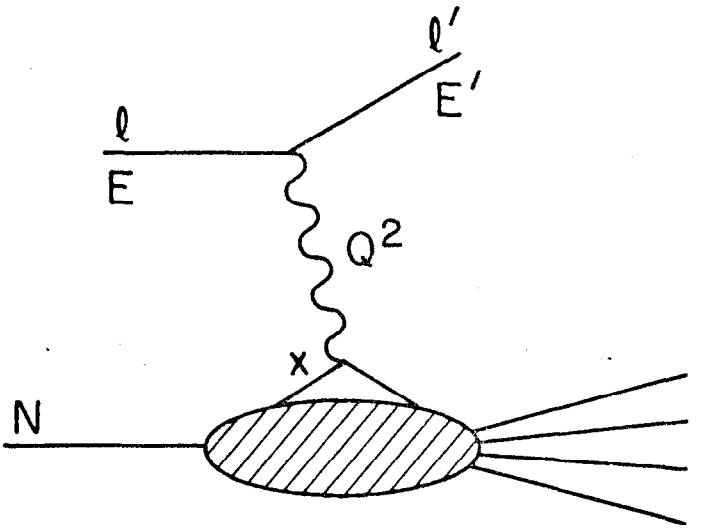

Fig. 6

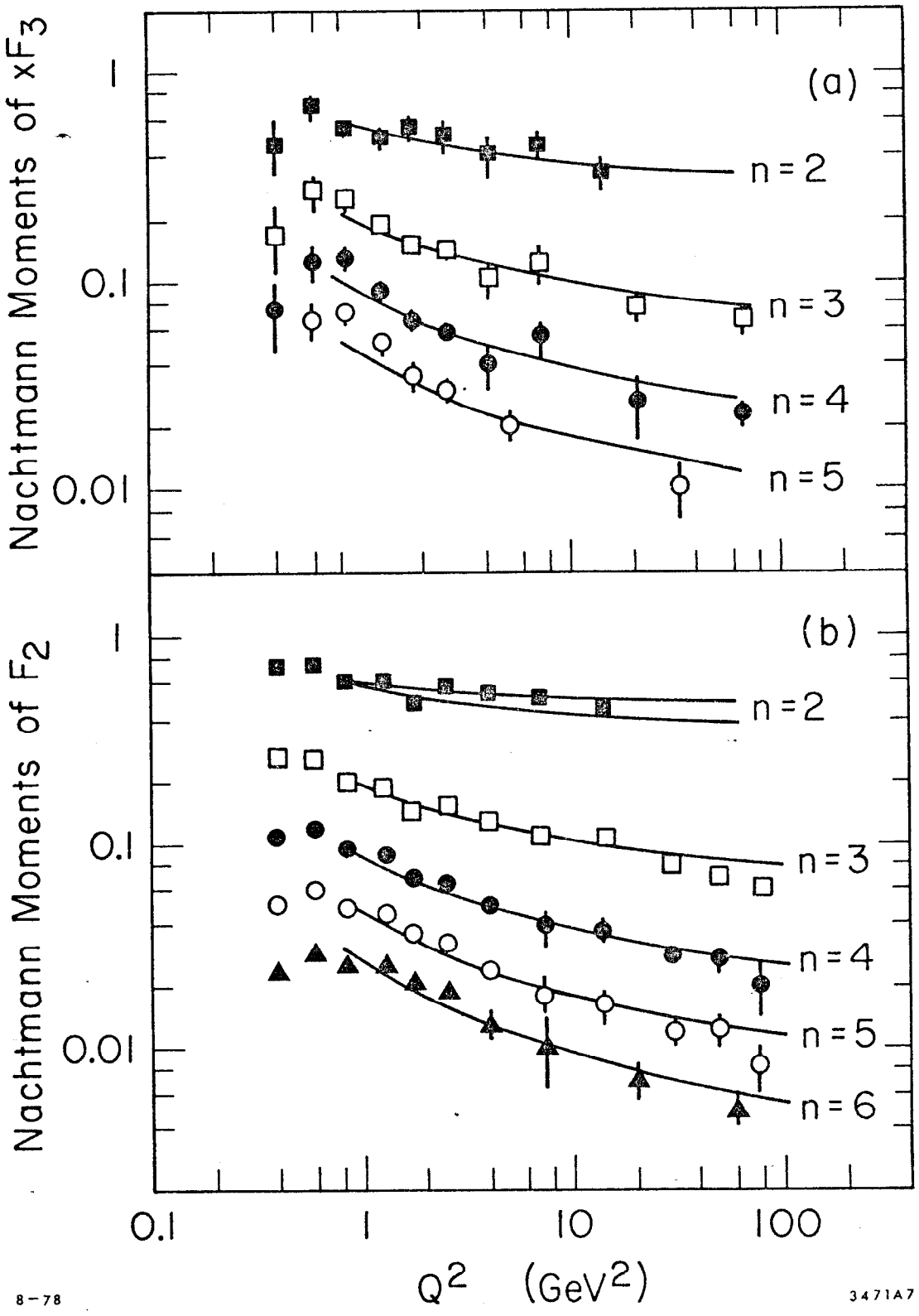
Nachtmann Moments of xF_3
(a)
n = 2
n = 3
n = 4
n = 5
Nachtmann Moments of F_2
(b)
n = 2
n = 3
n = 4
n = 5
n = 6
1
0.1
0.01
0.1
1
10
100
Q^2 (GeV^2)
8-78
3471A7

Fig. 7

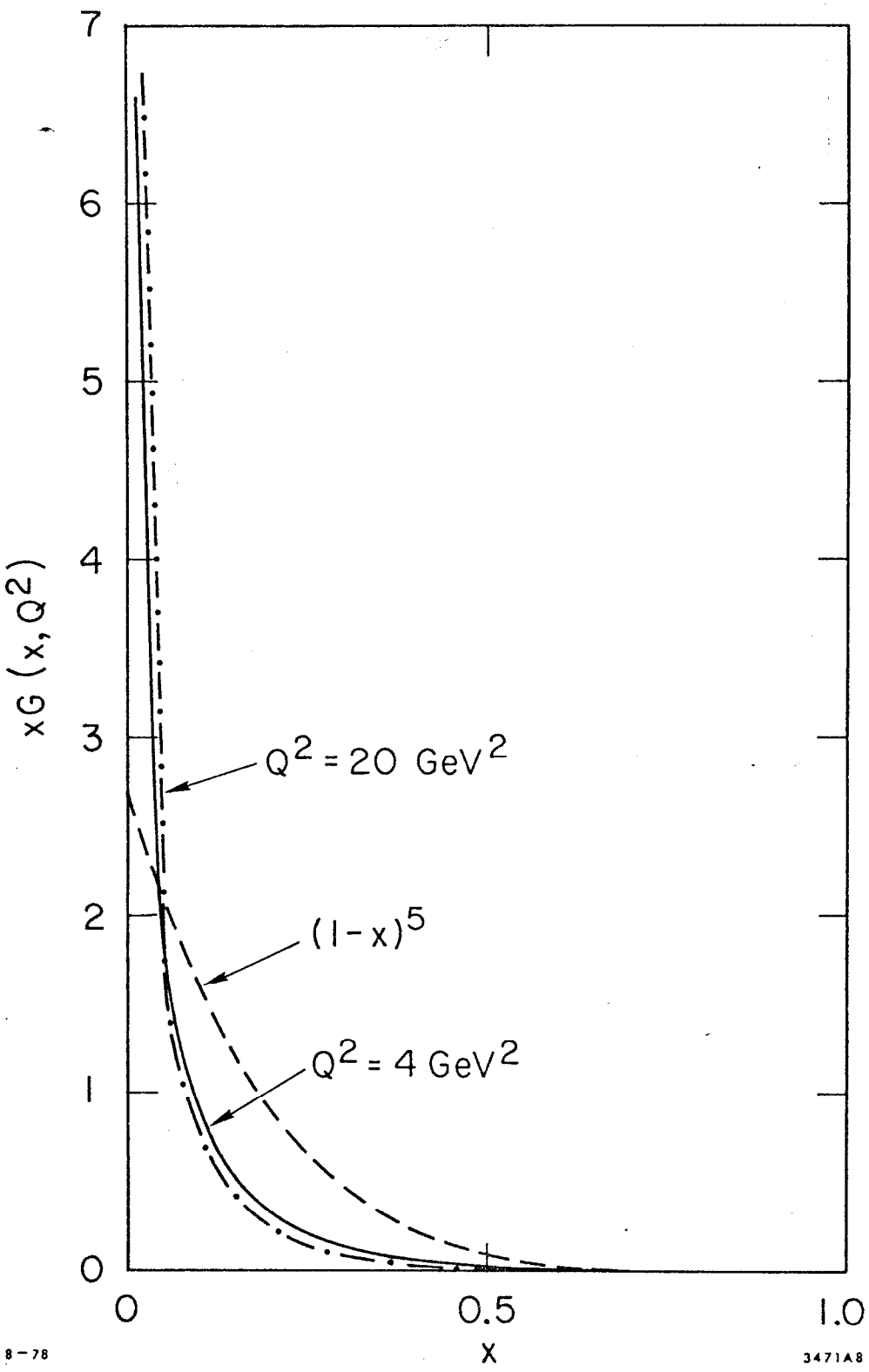

Fig. 8

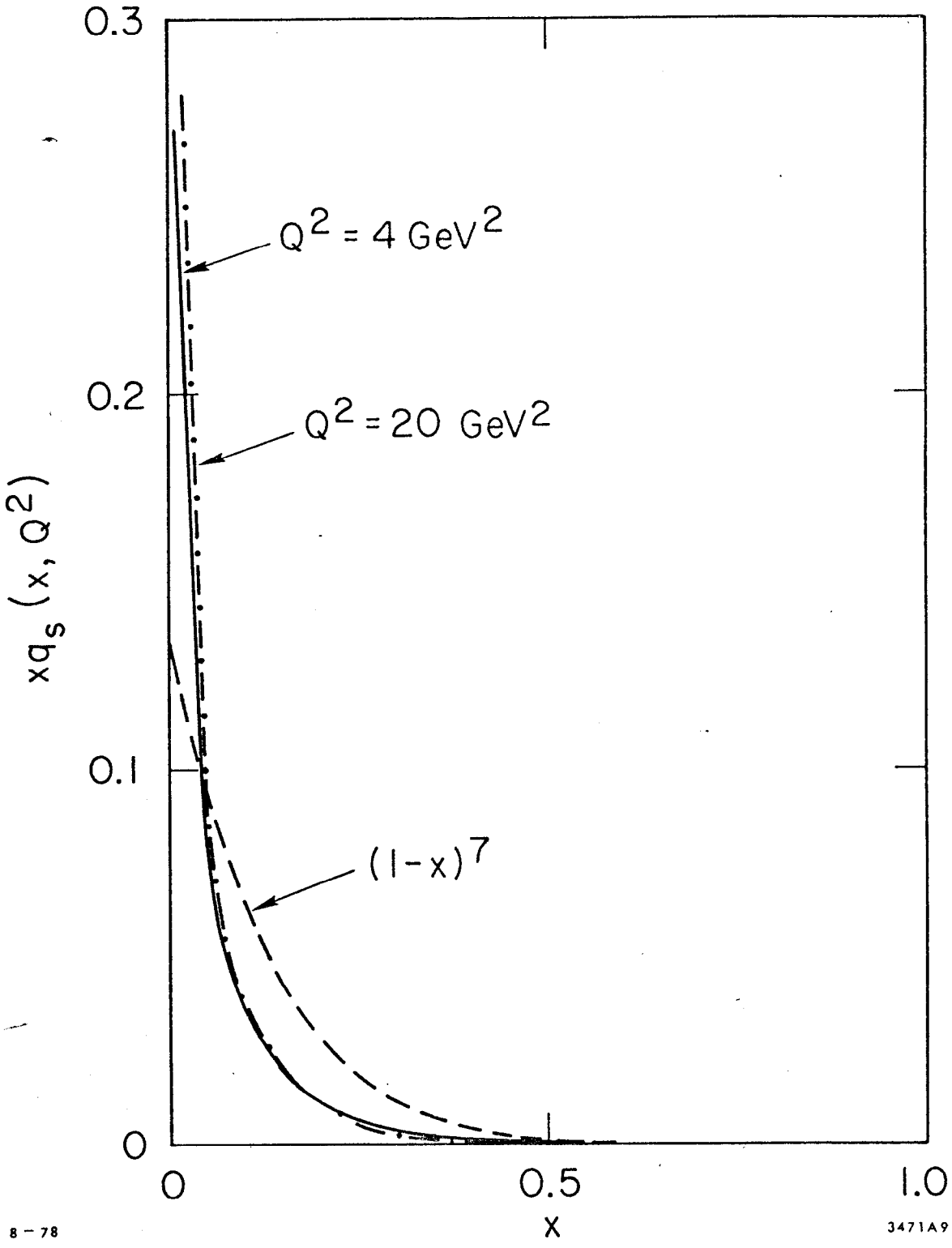

Fig. 9

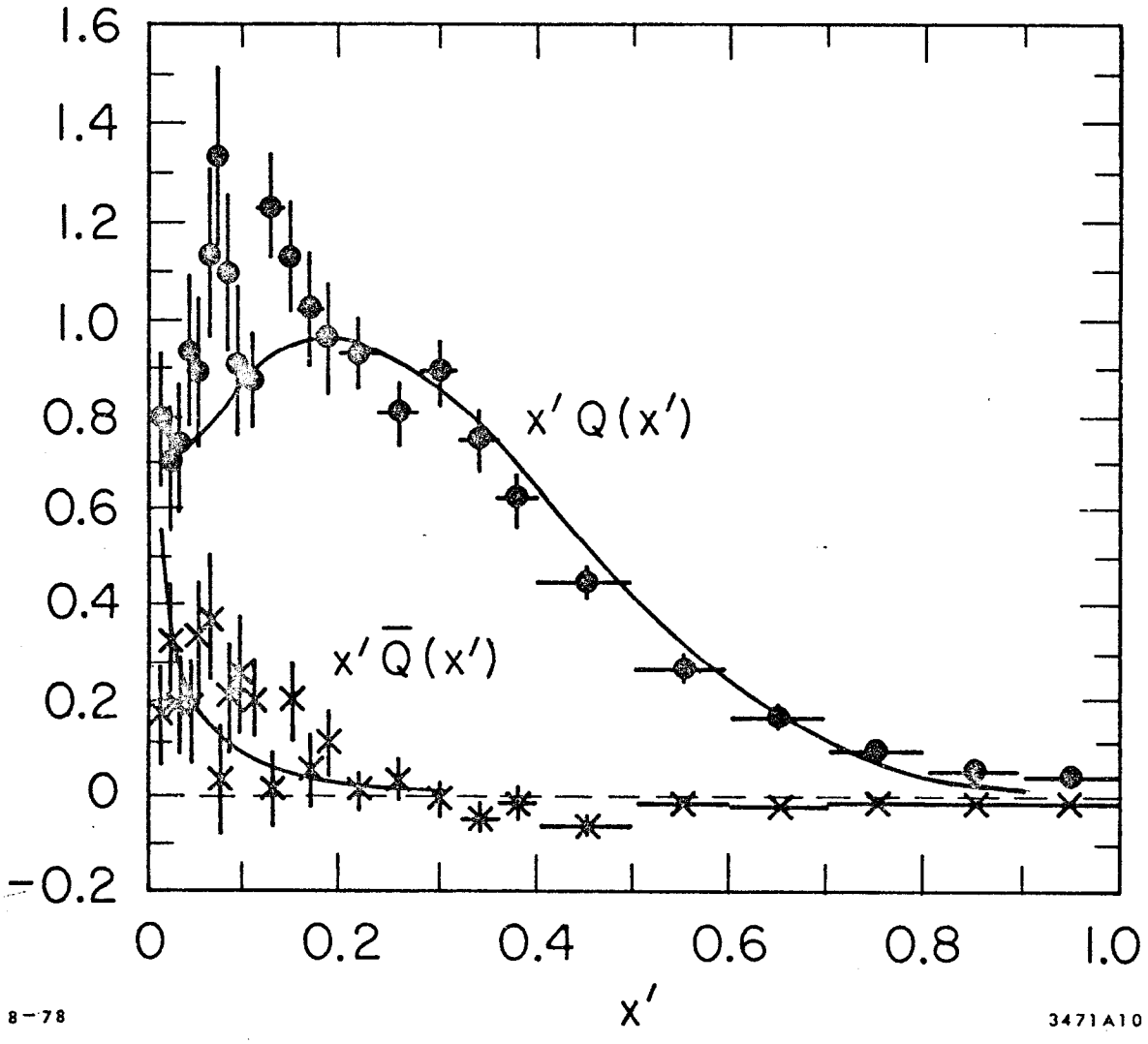

Fig. 10

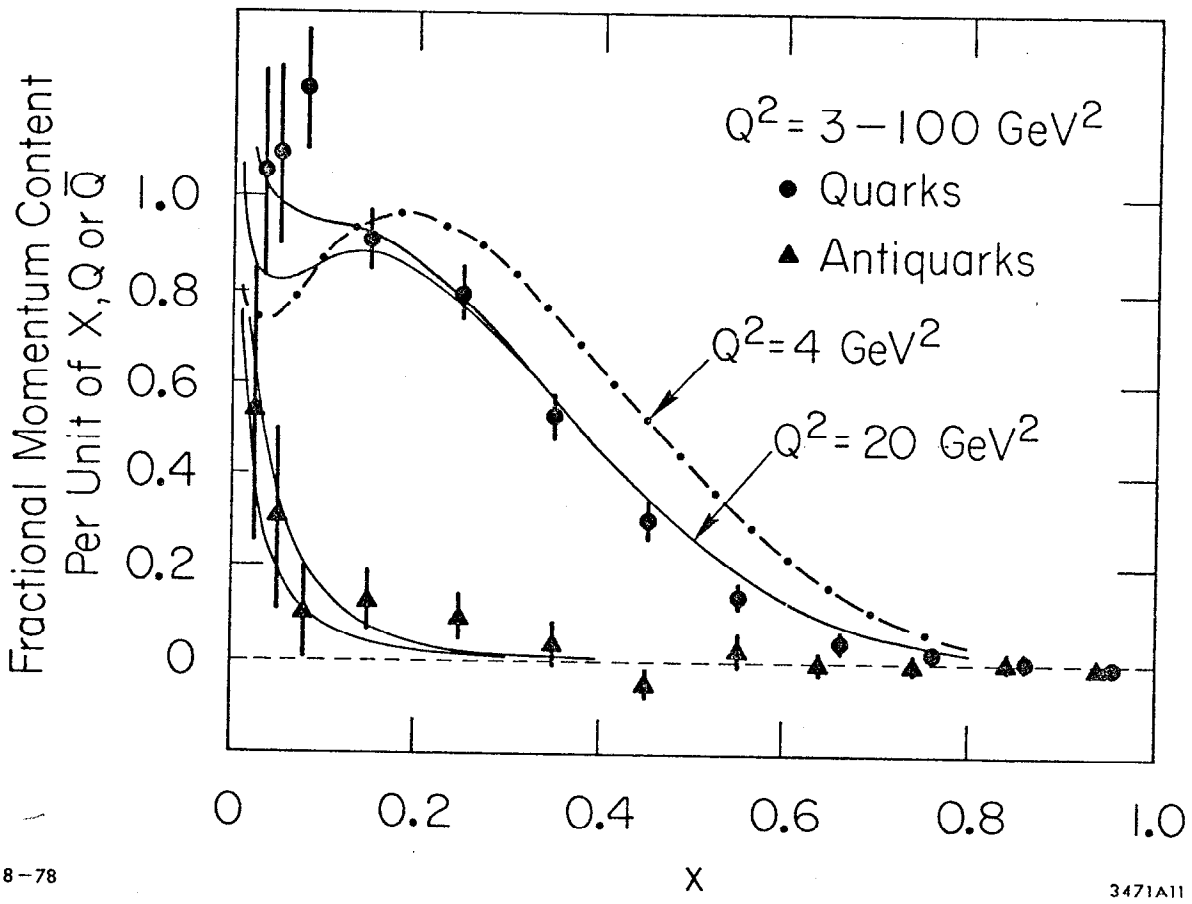
Fractional Momentum Content
Per Unit of X, Q or $\bar{Q}$
1.0
0.8
0.6
0.4
0.2
0
$Q^2 = 3-100$ GeV^2
Quarks
Antiquarks
$Q^2 = 4$ GeV^2
$Q^2 = 20$ GeV^2
0
0.2
0.4
0.6
0.8
1.0
X
8-78
3471A11

Fig. 11

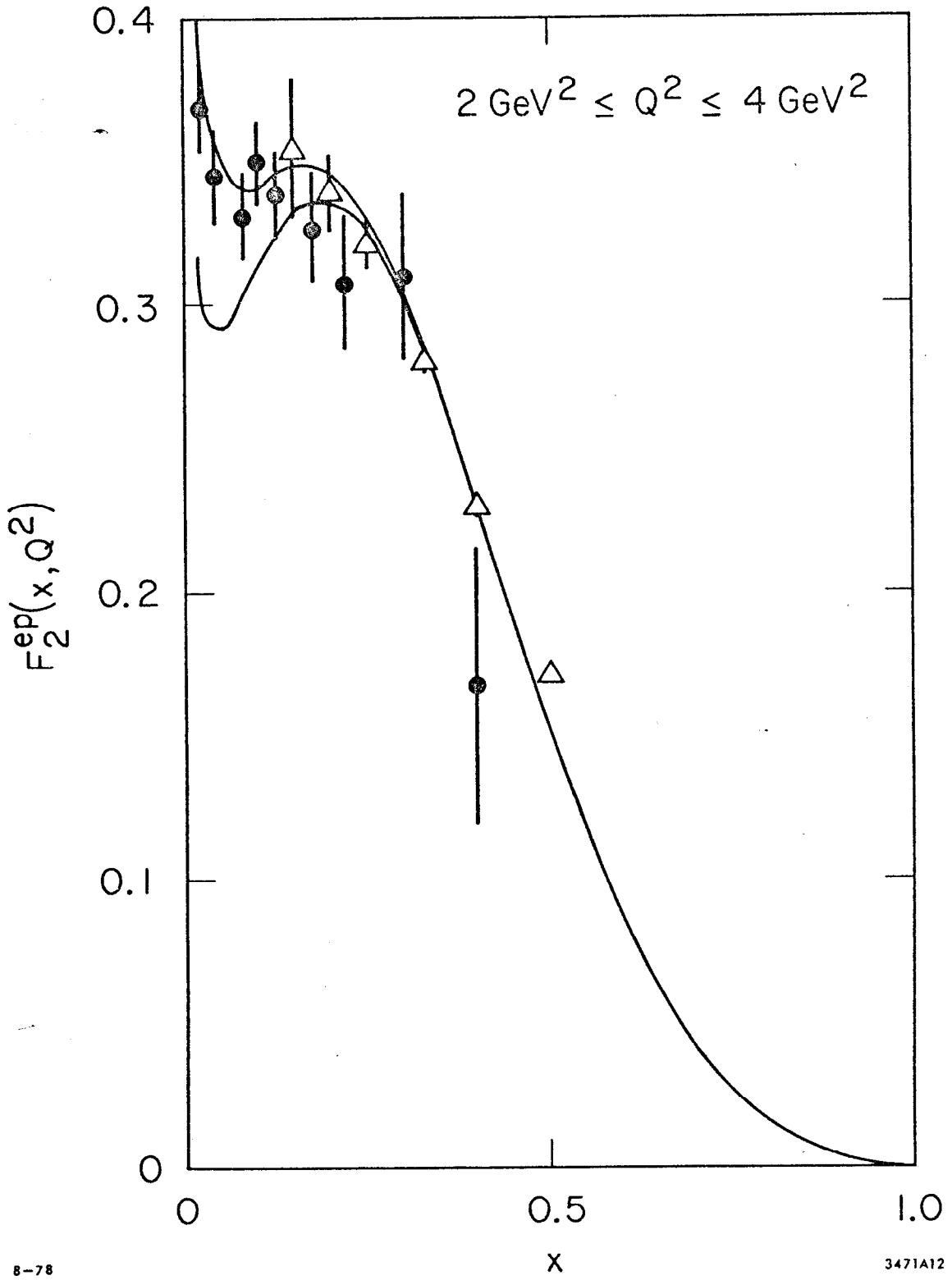
0.4
0.3
0.2
0.1
0
0
0.5
1.0
$2\ \mathrm{GeV}^2 \leq Q^2 \leq 4\ \mathrm{GeV}^2$
$F_2^{ep}(x, Q^2)$
x
8-78
3471A12

Fig. 12

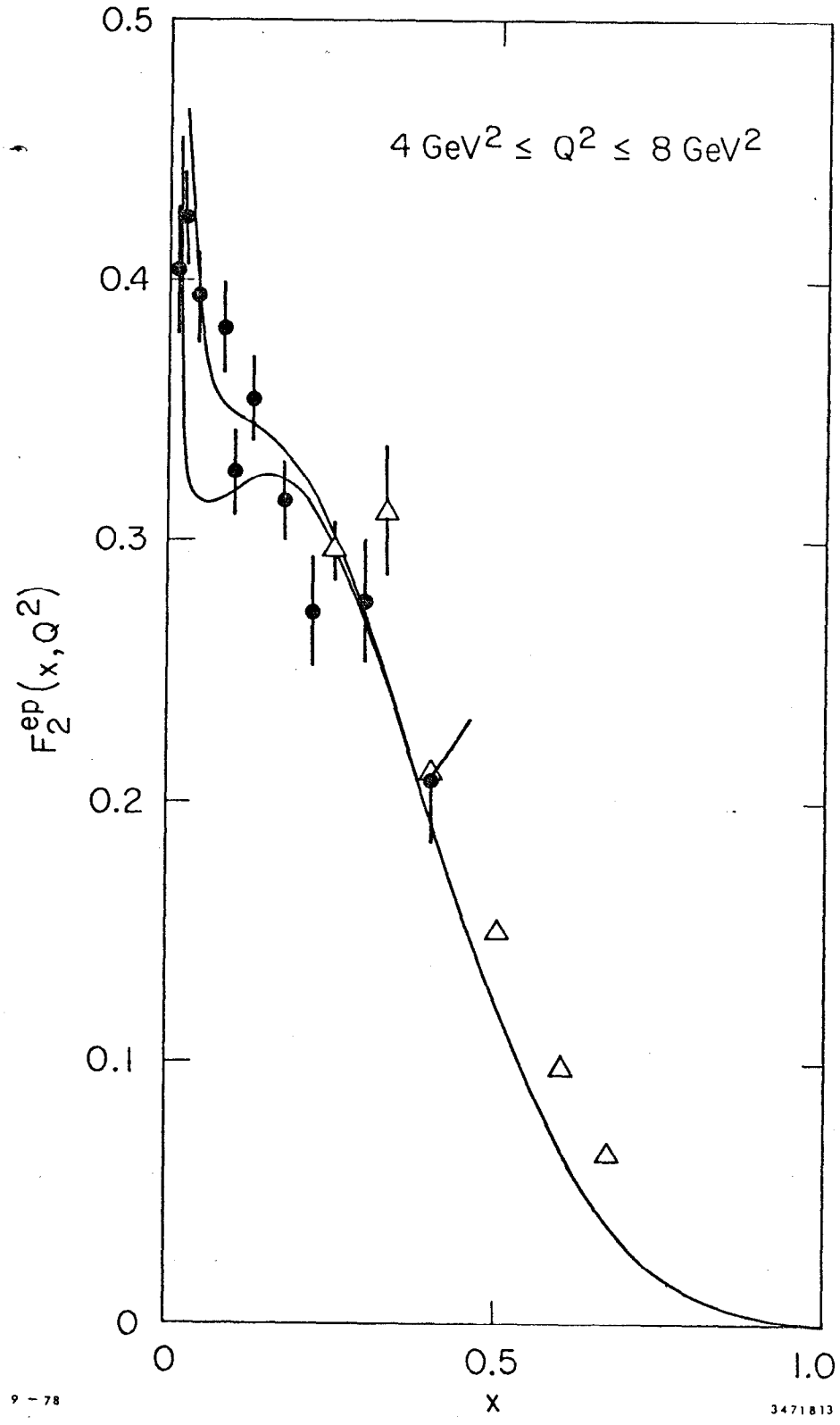
0.5
0.4
0.3
0.2
0.1
0
$4\ GeV^2 \leq Q^2 \leq 8\ GeV^2$
$F_2^{ep}(x, Q^2)$
0
0.5
1.0
x
9 – 78
3471813

Fig. 13

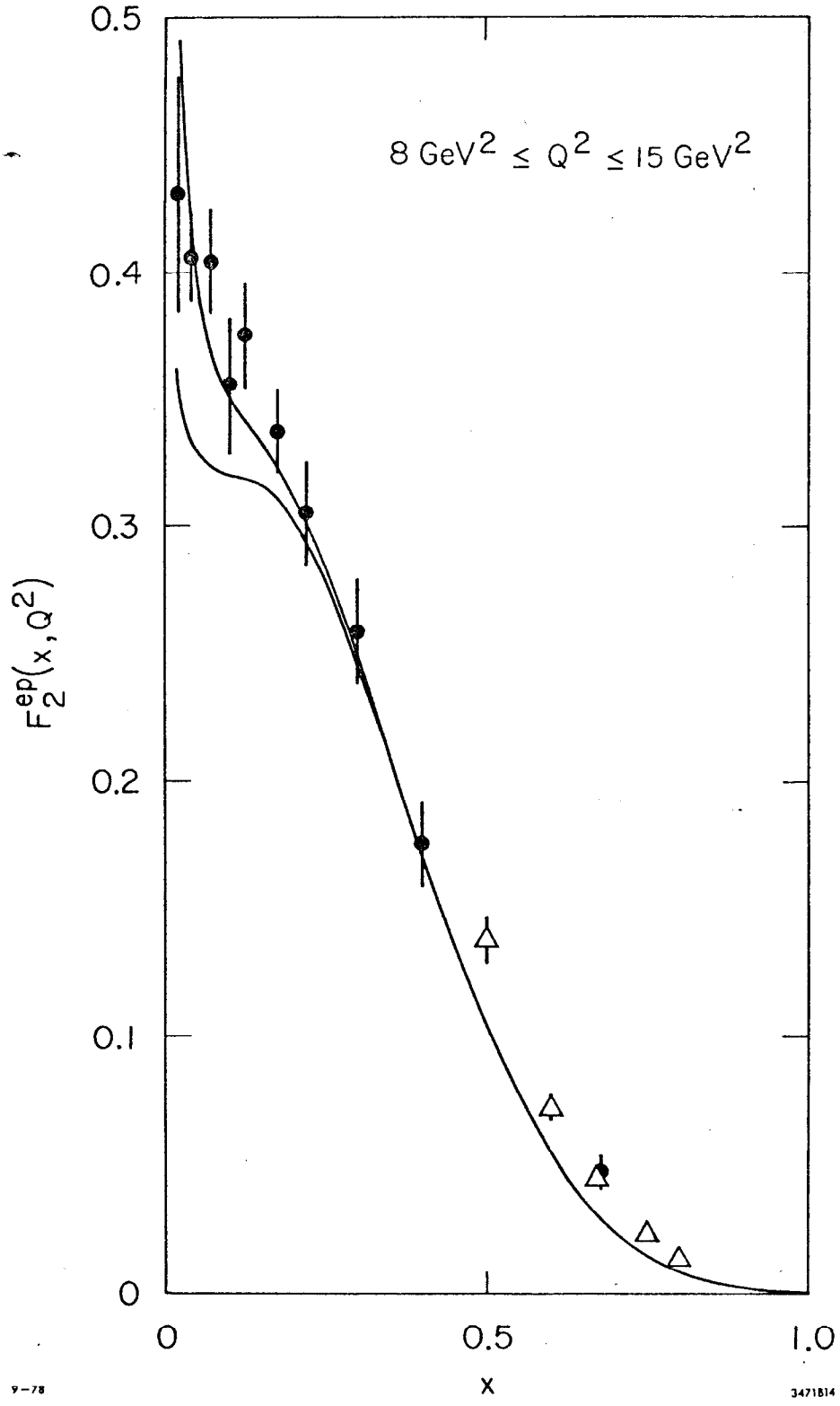
0.5
0.4
0.3
0.2
0.1
0
$8\ GeV^2 \leq Q^2 \leq 15\ GeV^2$
$F_2^{ep}(x,Q^2)$
0
0.5
1.0
x
9-78
3471B14

Fig. 14

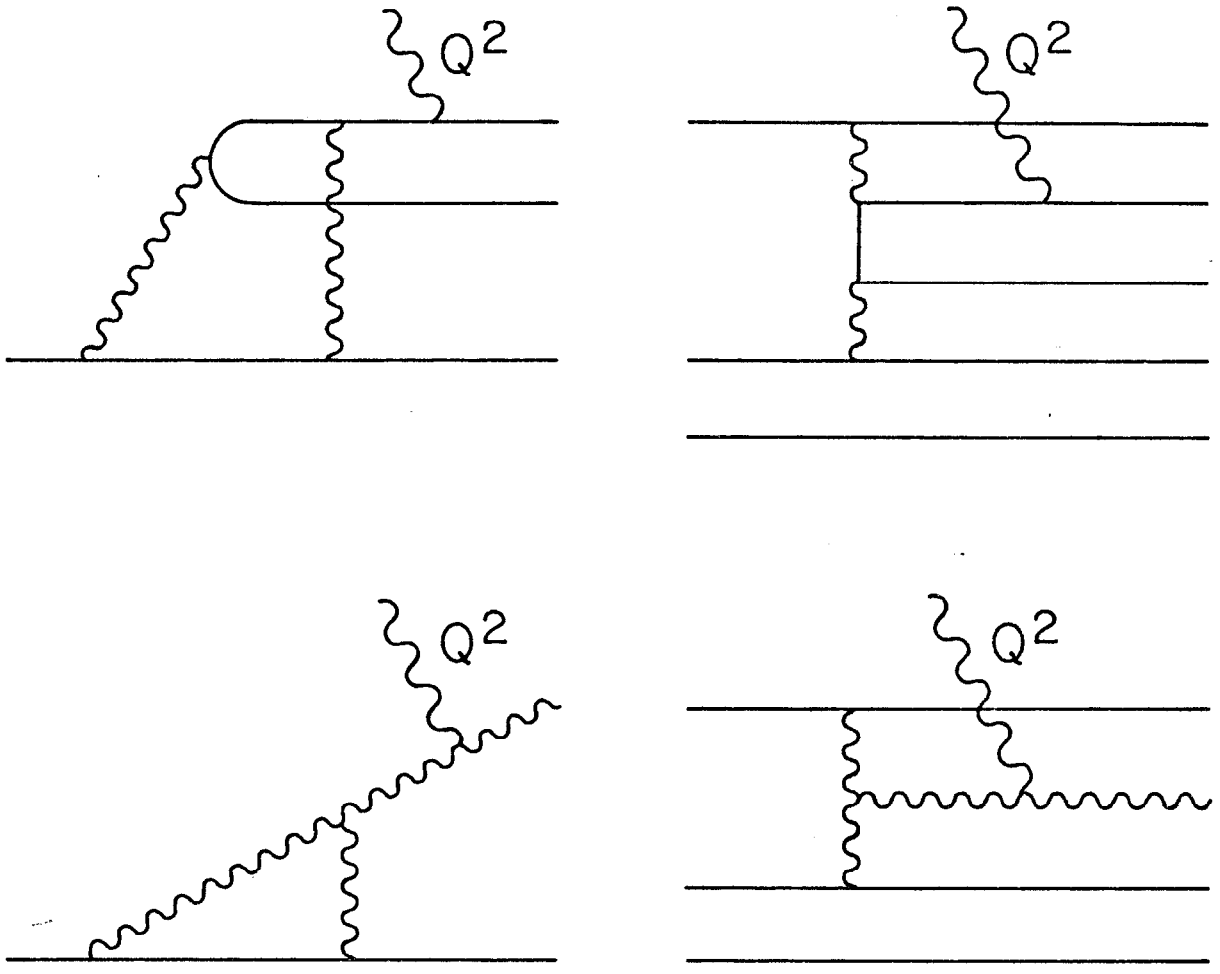

8–78

3471A15

Fig. 15